STM JOURNALS

Research & Reviews: Journal of
Computational Biology

https://journals.stmjournals.com/rrjocb

ISSN: 2319-3433 (Online)
ISSN: 2349-3720 (Print)
Volume 13, Issue 2, 2024
May–August
DOI (Journal): 10.37591/RRJoCB

Research RRJoCB

Exploring the Potential of *Allium sativum* Phytocompounds as B-Cell Leukemia 2 Inhibitors in Acute Lymphoblastic Leukemia: Molecular Docking Study

Santhiya K.[1,*]

Abstract

Objective: *Acute lymphoblastic leukemia (ALL) is a lymphoid progenitor cell malignancy that could be treated with plant-based drugs, thus alleviating the off-target effects caused by conventional chemotherapy. Since ancient days, Allium sativum has been an integral part of traditional medicine and an excellent antimicrobial, antioxidant, and antiproliferative agent. Hence, this study aims to assess the anti-leukemic potential of A. sativum phytoconstituents as the B-cell leukemia 2 protein (Bcl-2) natural inhibitor drug.* ***Methods:*** *25 phytoconstituents of A. sativum were subjected to screening of pharmacological properties, drug-likeliness, toxicity, and absorption, distribution, metabolism, and excretion (ADME) characteristics using SwissADME and ADMET 2.0 tools, respectively, for their potential to serve as drug leads or ligands. Bcl-2 protein, a B-cell apoptosis regulator, along with their homologous chains A, B, C, D, E, and F are extracted from the Protein Data Bank (PDB) and purified using the protein visualizer tool Discovery Studio. The A. sativum ligands and Bcl-2 target were docked by the PyRx tool.* ***Results:*** *The target protein stability and conformation were predicted by 93% percentage favored regions of amino acids in the Ramachandran plot obtained through different combinations of phi and psi angles. Overall, five ligands of A. sativum, namely kaempferol, quercetin, 1-ethylquinolinium iodide, carvacrol, and eugenol, had the best binding affinities with target protein Bcl-2 with acceptable ADME ranges and other properties, thereby promoting them as safe drug candidates.* ***Conclusion:*** *The renowned anti-cancerous properties of kaempferol, quercetin, 1-ethyl quinolinium iodide, carvacrol, and eugenol are proven to inhibit the Bcl-2 target protein in ALL through these molecular interactions.*

Keywords: *Allium sativum*, anti-leukemic, Bcl-2 protein, acute lymphoblastic leukemia, molecular docking, phytocompounds, ADME screening, Bcl-2 inhibitors

INTRODUCTION

Acute lymphoblastic leukemia (ALL) emerges as the uncontrollable proliferation of immature lymphoid progenitor cells occurring in the bone marrow, blood, and extramedullary sites. Around 80% of ALL occurs in childhood; however, its effects are detrimental when encountered in adults [1]. In the US, the occurrence rate of ALL is found to be 1.8 per 100,000 people each year from 2016 to 2020 [2]. Origin of ALL in the hematopoietic cells is from either B-cell precursors causing B-cell precursor ALL (BCP-ALL/B-ALL) or T-cell lineages (T-ALL). Analysis of the cellular immunophenotype of both types reveals genetic alterations as the illness-inducing lesions [3]. 85% of the childhood ALL are from B-cell lineage, with

***Author for Correspondence**
Santhiya K.
E-mail: santhiyakaruppieh@gmail.com

[1]Student, Department of Bioinformatics, Bionome, Bengaluru, Karnataka India

Received Date: September 17, 2024
Accepted Date: October 27, 2024
Published Date: November 04, 2024

Citation: Santhiya K. Exploring the Potential of *Allium sativum* Phytocompounds as B-Cell Leukemia 2 Inhibitors in Acute Lymphoblastic Leukemia: Molecular Docking Study. Journal of Computational Biology. 2024; 13(2): 53–80p.

BCP-ALL being the most common. Chromosomal fusions (ETV6-RUNX1) and aberrations like t (12;21) (p13; q22) account for about 25% of BCP-ALL incidence [4]. Apoptosis mediated through energy-dependent biochemical pathways is an important tumor-inhibiting strategy [5]. Normally, the mitochondrial functions are regulated to inhibit the oxidative phosphorylation and promote the release of pro-apoptotic proteins such as cytochrome c, B-cell leukemia 2 (Bcl-2) family, BCL2-antagonist-killer (Bak), and Bcl-2-associated X-protein (Bax) [6]. The Bcl-2 family proteins such as *BCL-2*, Bcl-extra-large *(BCL-XL)*, *BAX*, and *BAK* are highly important in apoptosis regulation in terms of their anti-apoptotic and pro-apoptotic effects. Among these, Bcl-2 is anti-apoptotic, while Bax is pro-apoptotic. Therefore, low Bax/Bcl-2 and high Bcl-2/Bax ratios indicating high relapse chances are paramount while devising the appropriate apoptotic therapeutic agent. The survival time of ALL patients obtained by analyzing the genetic polymorphism of Bcl-2 promoter regions provides dependable estimations than that of the Bax promoter regions. Thus, it is observed that Bcl-2 is a crucial determinant in the regulation of the B-cell intrinsic apoptotic pathway [7, 8]. *In vitro* studies on the CCRF-CEM cell line that is resistant to chemotherapy show increased doses of prednisolone induce cell death through upregulation of Bax gene expression and downregulation of Bcl-2 expression [9]. Prior research has shown the efficacy of Bcl-2 inhibitor drugs against ALL. ABT-737, a small-molecule Bcl-2 homology 3 (BH3) mimetic inhibitor of Bcl-2/Bcl-xL, is found to be anti-leukemic by initiating mitochondrial apoptosis [10].

The human Bcl-2 gene translocated between chromosomes 18 and 14 (t14;18) leads to a dysfunctional expression pattern leading to cancer [11, 12]. The binding interaction between the Bcl-2-like proteins and other pro-apoptotic establishes a balanced rheostat model of counteracting protein complexes that ultimately defines the cell fate [13]. Optimal dose stratification of chemotherapeutic agents has significantly enhanced remission-free survival in pediatric patients. However, these techniques still lead to poor prognosis in elderly patients, accounting for only 30–40% of individuals achieving long-term remission [14].

Allium sativum traces its origin to Central Asia and 5000-year-old folklore functional food, prophylactic, and therapeutic agent. Some of the well-studied anti-cancerous mechanisms of garlic include inhibition of mutations, scavenging of free radicals generated by oxidative stress, circumvention of anti-tumor activities like proliferation, resistance to apoptosis, and immunomonitoring escape [15]. This study is carried out to explore the anti-leukemic potential of *A. sativum* phytoconstituents as a nature-based alternative to conventional chemotherapeutic drugs.

MATERIALS AND METHODS

Network Interactions of Target Protein Bcl-2

The network interaction of Bcl-2 with other proteins was visualized in the STRING 11.5 software (https://string-db.org/). The purpose of the STRING database is to compile, rate, and combine data on protein-protein interactions from all publicly available sources through computational predictions. It provides a comprehensive and objective whole network with both direct or physical and indirect or functional interactions [16].

Preparation of Target Protein

The three-dimensional protein structure of an apoptosis regulator human Bcl-2 homo hexamer (PDB ID:4AQ3) was downloaded from the Research Collaboratory for Structural Bioinformatics Protein Data Bank (RCSB PDB) (*https://www.rcsb.org/*) [17, 18] in PDB format. Protein visualizer Discovery studio v24.1.0.23298 (BIOVIA) tool used to view the 3D structure of 4AQ3 and remove the water molecules, other co-crystals like ions, as well as ligands. Then clean protein was saved in PDB format for the upcoming docking analysis [19].

Preparation of *A. sativum* Phytocompounds/Ligands

Allium sativum (Figure 1) phytocompounds of root, rhizome, and bulb were extracted from the Indian medicinal plants, phytochemistry and therapeutics (IMPPAT) database, (https://cb.imsc.res.in/imppat.).

IMPPAT is a manually curated webserver that provides a list of phytoconstituents of Indian medicinal plants along with their therapeutic uses, physicochemical, ADMET, and drug-likeliness properties [20]. The respective 3D structures of phytocompounds in structured data file (SDF) and their canonical simplified molecular input line entry specification (canonical SMILES) for ADME analysis are derived from the PubChem database (https://pubchem.ncbi.nlm.nih.gov). PubChem is a widely used open-sourced public chemical database that gathers chemical information from more than 750 data domains. It has three sub-sets of databases namely, the substance, compound, and bioassay. The substance domain stores the depositor-driven chemical data. The compound page extracts the chemical structures from the structure database. The Bioassay is a collection of results of biological assays and experimental tests of the chemicals. Most of the Pubchem information is used for virtual screening of drugs, toxicity and drug-induced side effects prediction, metabolite analysis, and drug repurposing [21].

Evaluation of *In Silico* ADME Properties

Absorption, distribution, metabolism, and excretion (ADME) pharmacokinetic properties of the *A. sativum* ligands were examined for their drug-likeability using the SwissADME tool (http://www.swissadme.ch/). This webserver provides preliminary screening for ligands by analyzing their physicochemical properties, solubility, bioavailability, permeability, and other biological properties, such as lead-likeness, synthetic accessibility, Lipinski parameters, etc. [22].

Lipinski Rule

Drug-likeliness of ligands is determined by the Lipinski rules that include the range limit analysis of molecular weight, hydrogen donors, hydrogen acceptors, and partition coefficient which is an indicator of drug lipophilicity. The (Table 1) shows the acceptable range limits of Lipinski parameters, etc. [23].

Table 1. Parameters of Lipinksi filter.

S. N.	Ligand properties	Optimal range
1.	Molecular weight	< 500 Daltons
2	Hydrogen donors	< 5
3	Hydrogen acceptors	< 10
4	Partition coefficient (MlogP)	< 5

Physicochemical Properties

According to SwissADME analysis, the physicochemical parameters to be considered for easy internalization and enhancing the functionality of ligands include lipophilicity (XlogP), topological polar surface area (TPSA), saturation (Sp^3 hybridization), flexibility (rotatable bonds), and molar refractivity (MR) (Table 2) [22].

Figure 1. *Allium sativum.*

Table 2. Acceptable physicochemical ranges for ligands.

S. N	Properties	Optimal range
1	XLogP	-0.7–6.0
2	TPSA	20–130
3	Fraction Sp3 hybridization	>0.25
4	Number of rotatable bonds	< 9
5	Molar refractivity (MR)	40-130

Table 3. Toxicity categorization in ADMET2.0.

S.N.	Category	Toxicity level	Range limit
1	0	Low	> 500 mg/kg
2	1	High	< 500 mg/kg

Table 4. Empirical toxicity predicted by ADMET2.0.

S.N.	Empirical value	Color indicator	Empirical decision on toxicity
1	0-0.3	Green	Excellent/non-toxic
2	0.3-0.7	Yellow	Medium/moderately toxic
3	0.7-1.0 (++)	Red	Poor/highly toxic

Prediction of Ligand Toxicity

The ADMET2.0 (*https://admetmesh.scbdd.com/*) is an updated version of the ADMET lab web server. This tool provides details on the pharmacokinetics and toxicity properties of ligands, which is an essential part of medicinal chemistry to prevent failure of drug development. The median lethal dose (LD50) is a measure of dosage at which the drug administered either through oral, dermal, or inhalation routes will kill 50% of the test animals within 24 hours of exposure. In ADMET2.0, LD50 is indicated by the rat oral acute toxicity, which indicates category 0 and 1 for the low and high toxic nature of the ligands, respectively [24, 25]. Tables 3 and 4 show the toxicity categorization of compounds according to ADMET2.0.

Virtual Screening/Molecular Docking and Visualization

Virtual screening, or molecular docking, is a computational technique used to screen a library of compounds against potential target protein receptors. Python prescription 0.8 (PyRx 0.8) (https://pyrx.sourceforge.io/) is a virtual docking tool used to analyze the behavior of small molecules to the binding pockets of target receptors. This tool combines other open-source software such as Open Babel, Autodock, and Autodock Vina to carry out docking [26]. Recent studies focus on the ability of small-molecule phytocompounds to interact and bind with target protein receptors since docking of larger ligands poses serious challenges in terms of conformational and combinatorial complexities between ligand domains and target proteins, resulting in the subsequent modification of binding modes and scoring [27]. The macromolecular target Bcl-2 homo hexamer containing A, B, C, D, E, and F chains was selected for docking with 25 phytoconstituents/ligands of *A. sativum* to identify the potential drug candidates as Bcl-2 inhibitors for ALL. The entire target protein was involved in docking to determine the comprehensive and holistic behavior of protein-ligand interactions. Both the target protein and ligands were converted from their respective PDB format and SDF format into autodock Protein Data Bank, partial charge (Q), and atom type (T) (PDBQT) format. The following steps and molecular docking process were carried out in the PyRx 0.8 tool. Ligands were subjected to an energy minimization step to avoid clashes and other conformational changes during ligand-protein complex binding interactions. This is followed by the grid box generation for the entire target protein-ligand complex. The grid center coordinates of the purified Bcl-2 target homo hexamer with chains A, B, C, D, E, and F of PDB ID: 4AQ3 were fixed to X = 28.349 Y = 15.6298 Z = 21.4915 along with dimensions X = 25.0000 Y = 25.0000 Z = 25.0000 in Angstroms. The molecular docking results saved in the comma-separated value (CSV) file format were analyzed for the best-docked target protein-ligand complexes with the highest log value of binding affinities, root mean square deviation upper boundary (RMSD UB), and root mean square deviation lower boundary (RMSD LB). The PDB format of selected ligands was downloaded from PyRx and visualized their 3D and 2D interactions with target proteins in the Discovery Studio v24.1.0.23298 (BIOVIA) tool.

RESULTS

Visualization of Target Protein Interactions

Figure 2 shows the STRING 11.5 results of network interactions. Bcl-2 binds with protein BAD, a pro-apoptotic factor that dimerizes with anti-apoptotic proteins Bcl-2 and Bcl-XL. BCL2-associated agonists of cell death (BAD) can inhibit the cellular protective effects of death suppressors Bcl-2 and Bcl-XL when they are coexpressed [28, 29]. The Bax, BCL2-antagonist-killer 1 (BAK1), Bcl-2 interacting mediator of cell death [BIM/Bcl-2-like 11 (BCL2L11)], NOXA (phorbol-12-myristate-13-acetate-induced protein 1 (PMAIP1)) and BCL2 interacting killer (BIK) proteins range in size between 100–200 amino acids and contain the BH-3 motif, which is essential to maintain their pro-death activities. They bind their BH-3 helix into the hydrophobic groove of anti-apoptotic Bcl-2 specifically to promote cell death [30]. The overexpression and interaction of anti-apoptotic factors like Bcl-2 and Bcl2L1 cause increased cell death and autophagy [31]. The Bcl-2 and beclin1 (BECN1) interactions are known to regulate autophagy. The network of anti-apoptotic Bcl-2 and autophagy initiator BECN1 stops the assembly of pre-autophagosomal structures, thereby preventing autophagy [32]. Though the Bcl-2 nineteen kilodalton interacting protein (BNIP3) belongs to the BH 3 only-containing protein subfamily like BIM, BIK, and NOXA, it cannot induce cell death by binding its BH3 domain with that of the anti-apoptotic Bcl-2 and Bcl-XL proteins through deletion of its transmembrane (TM) domain and the subsequent loss of homodimerization [33]. The tumor protein (TP53) pro-apoptotic factor interacts with the Bcl-2 protein and suppresses the latter's functions to trigger apoptosis and inhibit autophagy in the cytoplasm [34].

Purification of Target Protein/Macromolecule

The target macromolecule Bcl-2 was expressed by the gene hsa: 596 according to the Kyoto Encyclopedia of Genes and Genomes (KEGG) database (https://www.genome.jp/kegg/) [35]. At 2.40 Å resolution, X-ray diffraction studies derived the 3D structure of protein human Bcl-2 protein attached to the phenylacylsulfonamide inhibitor was downloaded from RCSB PDB database on PDB ID: 4AQ3 (PDB DOI: https://doi.org/10.2210/pdb4AQ3/pdb) in the PDB format. The target protein was purified for the attached ligand molecule phenylacylsulfonamide inhibitor and other heteroatoms in the BIOVIA Discovery Studio Visualizer, as shown in Figure 3.

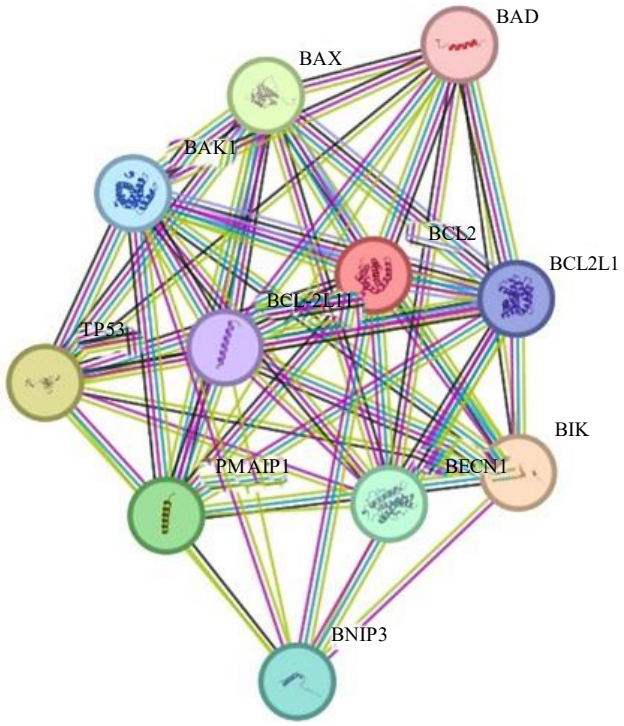

Figure 2. Bcl-2 interactions with other proteins as shown by STRING 11.5.

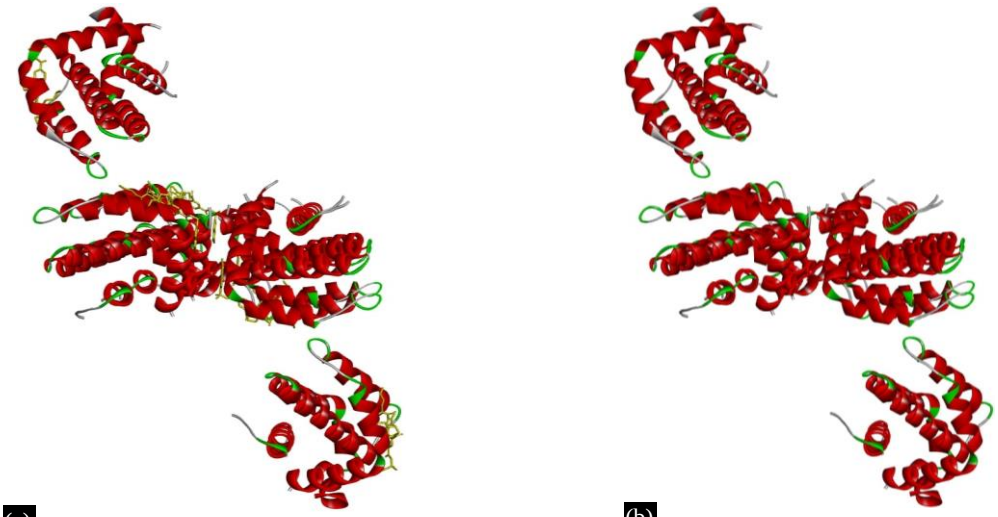

Figure 3. 3D structure of target protein Bcl-2 visualized in BIOVIA. (a) Bcl-2 with heteroatoms attached; (b) Bcl-2 with heteroatoms removed.

Structures of the Chosen Phytocompounds/Ligands

25 phytoconstituents of *A. sativum* were subjected to docking analysis. Out of them, 3D structures of the top five ligands, namely kaempferol, quercetin, 1-ethyl quinolinium iodide, carvacrol, and eugenol, with strong binding affinities to target protein Bcl-2 are shown in Figure 4(a), (b), (c), (d), and (e). Table 5 lists the binding affinities of selected ligands with Bcl-2.

Table 5. Top 5 ligands and their binding affinities with the target protein.

S.N.	Ligands	Binding affinity
1	Kaempferol	-7.9
2	Quercetin	-7.7
3	1-Ethylquinolinium iodide	-7.7
4	Carvacrol	-7.5
5	Eugenol	-7.3

Secondary Structure Analysis of Protein

The 3D and 2D structural information of Bcl-2 was collected from the pictorial 3D structures database of Protein Data Bank (PDBsum) (*https://www.ebi.ac.uk/thornton-srv/databases/pdbsum/*) [36]. The entire sequence length of Bcl-2 has 169 amino acid residues. The chains A, B, C, D, E, and F are identical to each other. The secondary structure of Bcl-2 contains 8 helices, 24 helix-helix interactions, and 5 beta turns. In addition, mutational variation of glycine and serine interchange was also observed at the 162 position, as shown in Figure 5.

Protein-Protein Interface Interactions: A}{C, E}{F, A}{D, A}{E, B}{D, B}{E

In total, six protein-protein interactions were observed among the A, B, C, D, E, and F chains of Bcl-2 protein in the PDBsum software, as displayed in Figure 6. In A}{C interaction, the A chain has 6 interface residues with an interface area (Å^2) 289, while the C chain has 4 interface residues with an area of 333 Å^2 and are joined by 11 non-bonded or atomic contacts (Figure 6(a)). Between the E}{F network, the E chain has 8 interfacial atomic residues covering a 292 Å^2 area, joined with the F chain having 5 interface residues in an area of 366 Å^2 through 1 hydrogen bond and 34 non-bonded contacts (Figure 6(b)). In the case of A}{D, both A and D chains have 4 interfacial amino acid residues each with areas of 228 Å^2 and 209 Å^2, respectively. This interaction is established by 2 hydrogen bonds and 15 non-bonded contacts (Figure 6(c)). A}{E interaction has A chain having 11 interfacial residues with

532 Å^2 area, and the E chain with 9 residues and an area of 548 Å^2 connected by 4 hydrogen bonds and 52 non-bonded contacts (Figure 6(d)). B}{D network are joined together by 4 hydrogen bonds and 50 non-bonded contacts, where the B and D chains each have 10 interfacial amino acid residues with 565 Å^2 and 560 Å^2 interfacial areas respectively (Figure 6(e)). The B chain with 3 interfacial residues and an area of 269 Å^2 and the E chain with 4 interfacial residues and 253 Å^2 area are connected by 2 hydrogen bonds and 11 non-bonded contacts in the B}{E protein-protein interface (Figure 6(f)). None of the above interactions have salt bridges or disulfide bonds.

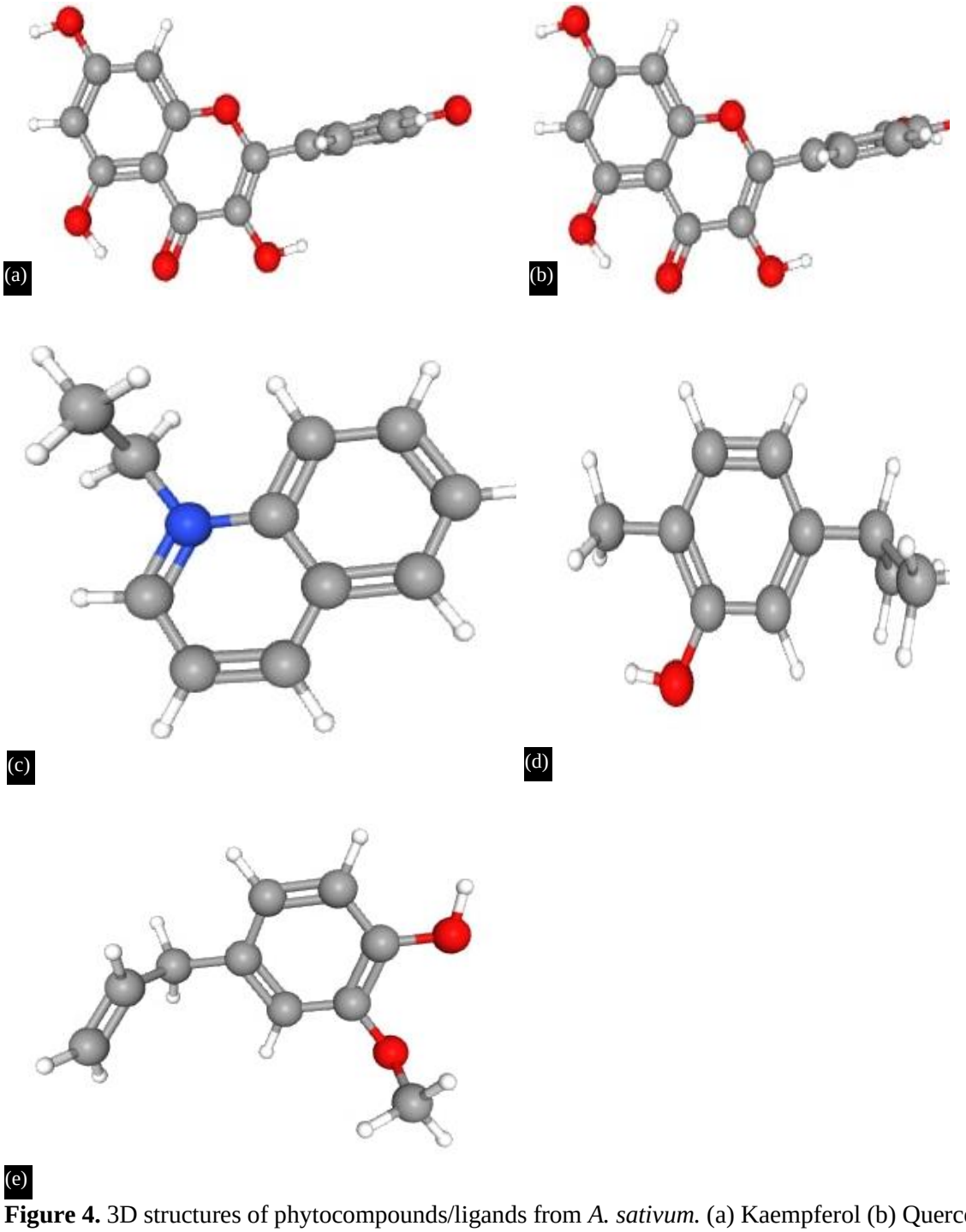

Figure 4. 3D structures of phytocompounds/ligands from *A. sativum.* (a) Kaempferol (b) Quercetin (c) 1-Ethylquinolinium iodide (d) Carvacrol (e) Eugenol.

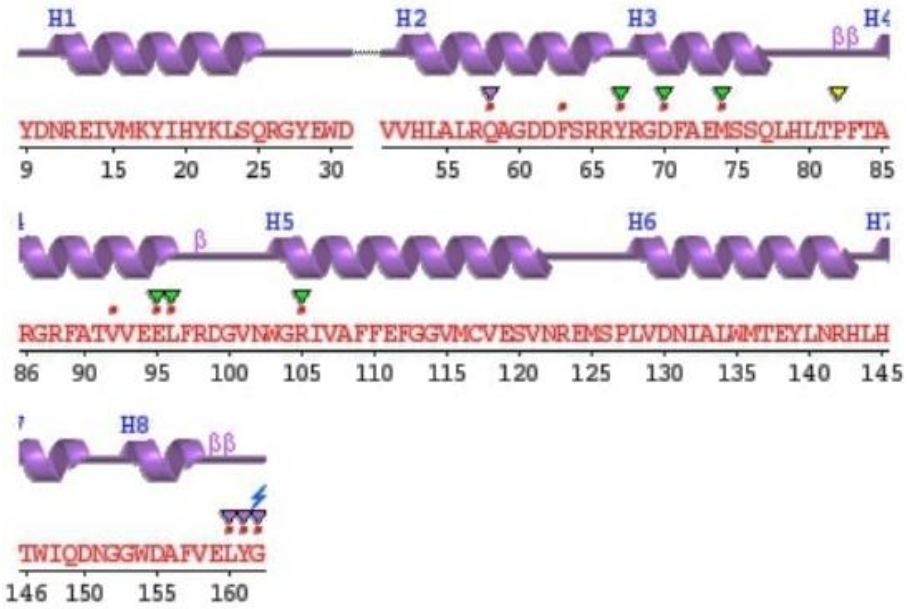

Figure 5. Secondary structure of target protein Bcl-2 in PDBSUM.

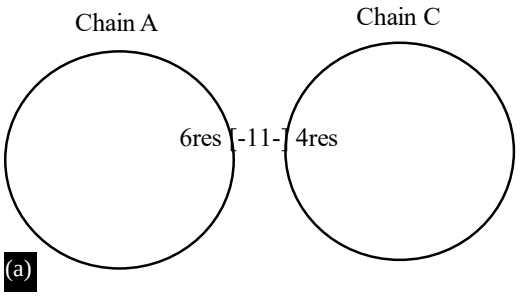

A}{C chain interactions with 11 non-bonded contacts.

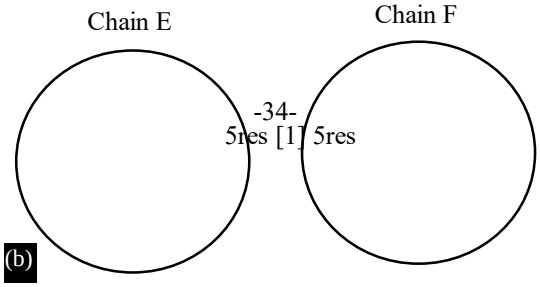

E}{F chain interactions with a hydrogen bond and 34 non-bonded contacts.

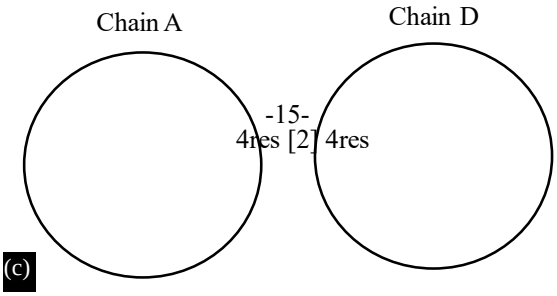

A}{D chain interactions with 2 hydrogen bonds and 15 non-bonded contacts.

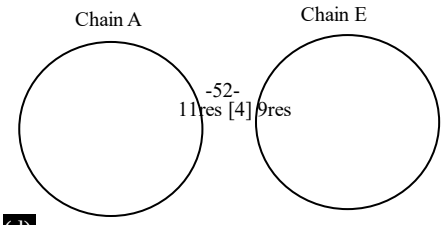

(d)

A}{E chain interactions with 4 hydrogen bonds and 52 non-bonded contacts.

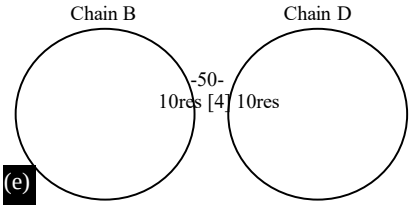

(e)

B}{D chain interactions with 4 hydrogen bonds and 50 non-bonded contacts.

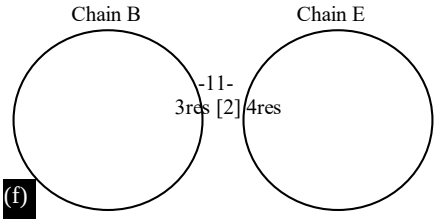

(f)

B}{E chain interactions with 2 hydrogen bonds and 11 non-bonded contacts.

Figure 6. Protein-protein interfacial interactions between the A, B, C, D, E, and F chains of Bcl-2.

Structural Assessment Through Ramachandran Plot

The Ramachandran plot provides a structural quality assessment of protein secondary structure through the phi and psi torsion angle combination and the corresponding localization of amino acids in the quadrant plot. The Ramachandran plot was generated in the PDBsum and PROCHECK analysis was performed as shown in Figure 7. The statistical data revealed the following information. On a total of 814 residues, the number of glycine and proline residues was 66 and 12, respectively. 18 end residues were shown excluding the glycine and proline. Out of the 718 non-glycine and non-proline residues, 667 residues present in the A, B, and L most favored regions (red colored), covering 92.9% of total residues, 49 residues (6.8% in yellow colored) seen in the additionally allowed regions a, b, l, and p, and no residues were found in the generously allowed region ~a,~b,~l,~p (mild yellow colored). Lastly, 2 residues (GLU 50 and TYR 161, accounting for 0.3% in the fourth quadrant) were found in the disallowed regions. According to the Ramachandran rule, a good protein model is expected to have over 90% amino acids in the favored region. Hence, with 93% favorable regions, the secondary structure of target protein Bcl-2 is Ramachandran favored.

Hydropathy Plot

The hydropathy plot identifies the number of hydrophobic amino acids in the protein Bcl-2 target. Proteins with 20–30 highly hydrophobic amino acids can span the entire lipid bilayer, as α-helix and hydrophilic amino acids aligned outside contribute to the conformation and stability of the cell membrane [37]. Emboss Pepwindow (*https://www.ebi.ac.uk/jdispatcher/seqstats/emboss_pepwindow*) software provides sequence statistics in terms of a hydropathy plot [38]. In the plot, the Y-axis is depicted by the hydrophobicity score, and the X-axis is depicted by amino acids in Figure 8. The hydrophobic nature of amino acids is indicated by a 0 to positive number, while the hydrophilic nature of amino acids is indicated by a 0 to negative value in the hydropathy plot. Figure 8 shows 7 peaks with hydropathy values 0 and above and 7 peaks with scores below 0, thereby indicating a neutral hydrophobic/hydrophilic ratio of amino acids.

Bcl-2 Protein Statistical Analysis

Bcl-2 target protein statistics were observed in the EMBOSS Pepstats (*https://www.ebi.ac.uk/jdispatcher/seqstats/emboss_pepstats*) software suite that provides various protein statistics for the prediction of functional characteristics. The Bcl-2 molecular weight is 19485.67, the average residue weight is 115.300, the charge is -6.5, and the isoelectric point is 4.9090. Table 6 shows the classification of amino acid residues along with their total number and molar percentage, obtained through EMBOSS Pepstats.

Analysis of ADME Properties

The ADME properties of ligands were examined by the SwissADME software and listed as shown in Table 7. Criteria such as GI absorption, BBB permeation, and P-glycoprotein (PGP) were considered for ADME analysis. Good GI absorption of drugs can increase the efficacy and oral bioavailability of drugs [39]. Major anti-cancer compounds such as carvacrol, eugenol, quercetin, and kaempferol have high GI absorption that corresponds to increased bioavailability. Generally, BBB permeation of drug ligands should be lower lest the ligands are intended for use in neurological therapy.

Evaluation of Lipinski Rules

Lipinski drug-likeliness parameters were calculated for all the phytocompounds by SwissADME as shown in Table 8 as per the properties in Table 1. 24 ligands taken for analysis fulfill the four Lipinski criteria, including molecular weight, hydrogen donors, hydrogen acceptors, and partial coefficient except octadecane, which has an MlogP value of 6.92 (Lipinski rule: MlogP < 5) while meeting the other 4 Lipinski requirements. Since only the partial coefficient value accounting for drug lipophilicity is slightly above the optimal range for octadecane, it was also included for analysis along with other phytoconstituents.

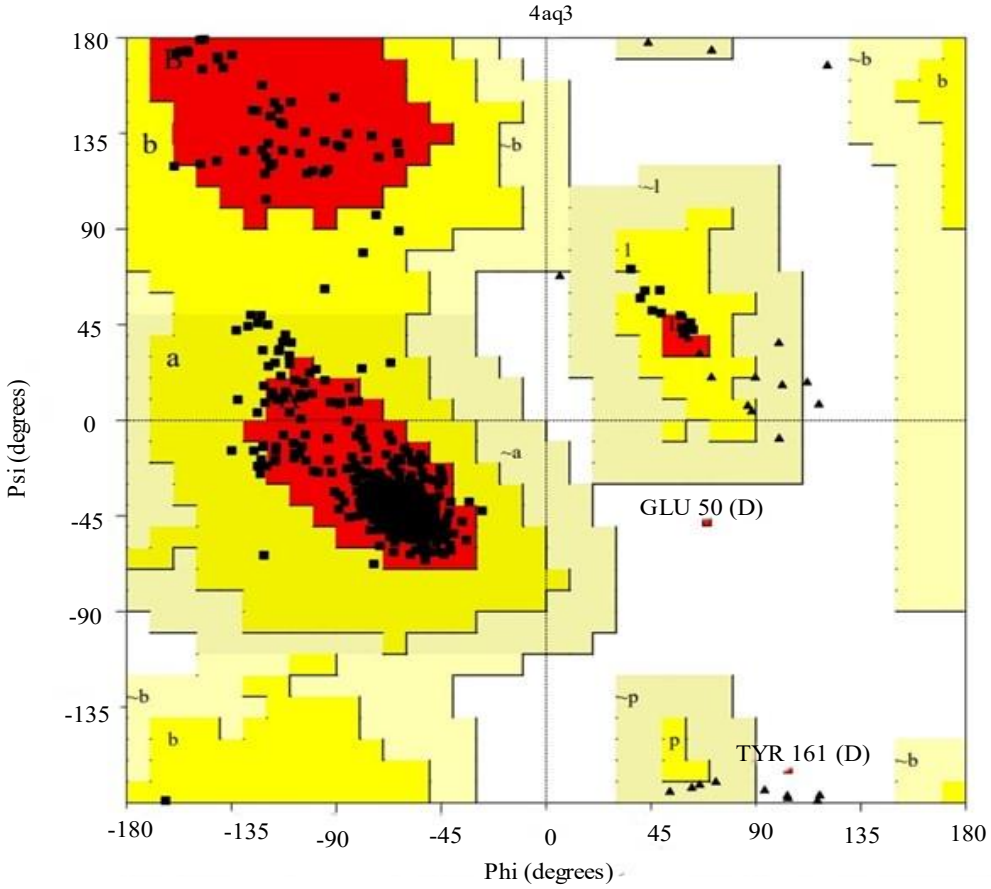

Figure 7. Ramachandran plot of Bcl-2 protein obtained through PROCHECK.

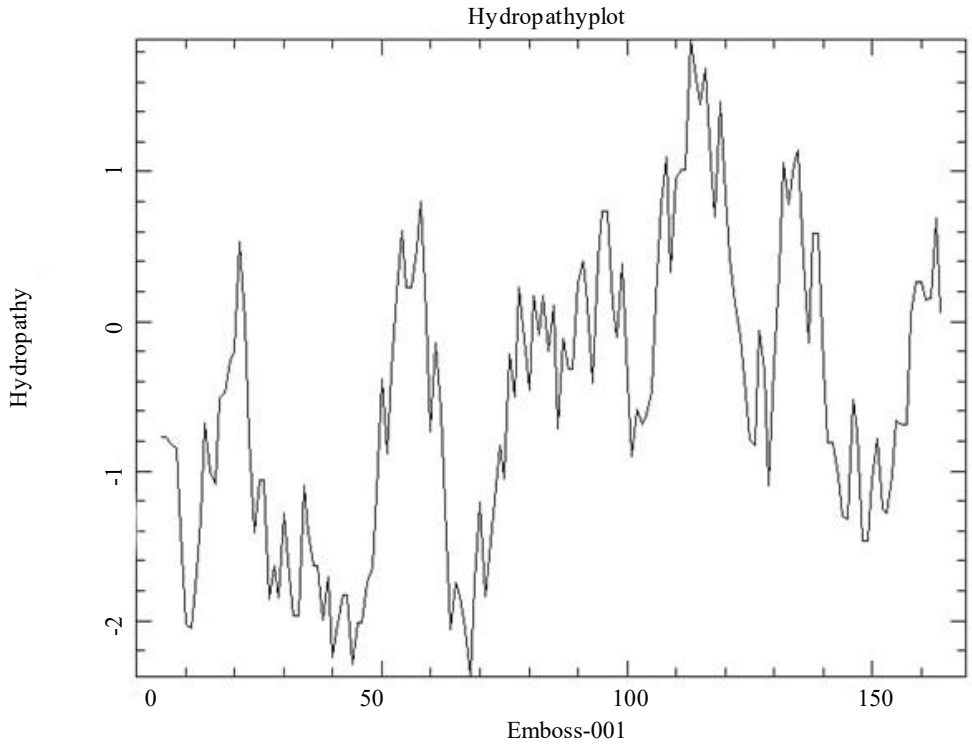

Figure 8. Hydropathy plot of Bcl-2 target by EMBOSS Pepwindow.

Table 6. Bcl-2 protein statistical analysis by EMBOSS Pepstats.

S. N.	Properties	Residues	Number	Mole %
1	Tiny	(A+C+G+S+T)	46	27.219
2	Small	(A+B+C+D+G+N+P+S+T+V)	81	47.929
3	Aliphatic	(A+I+L+V)	41	24.260
4	Aromatic	(F+H+W+Y)	28	16.565
5	Non-polar	(A+C+F+G+I+L+M+P+V+W+Y)	90	53.254
6	Polar	(D+E+H+K+N+Q+R+S+T+Z)	79	46.746
7	Charged	(B+D+E+H+K+R+Z)	24	30.178
8	Basic	(H+K+R)	24	14.201
9	Acidic	(B+D+E+Z)	27	15.976

Table 7. ADME properties of *Allium sativum* ligands obtained using SwissADME.

S.N.	Ligand	BBB permeation	GI absorption	PGP substrate	Solubility (Silicos-IT LogSw)
1	1-Propenyl allyl thiosulfinate	Yes	High	No	-1.07 (soluble)
2	Carvacrol	Yes	High	No	-3.01 (soluble)
3	Octadecane	No	Low	No	-7.13 (poorly soluble)
4	Allyl propyl disulfide	Yes	High	No	-2.13 (soluble)
5	Phenylacetic acid	Yes	High	No	-2.14 (soluble)
6	1-Ethylquinolinium iodide	No	Low	No	-3.66 (soluble)
7	Diallyl sulfide	Yes	High	No	-1.64 (soluble)
8	Dimethyl disulfide	Yes	High	No	-0.79 (soluble)
9	Eugenol	Yes	High	No	-2.79 (soluble)
10	Quercetin	No	High	No	-3.24 (soluble)

11	Diallyl trisulfide	Yes	High	No	-1.91 (soluble)
12	Dimethyl trisulfide	Yes	High	No	-0.94 (soluble)
13	Diallyl tetrasulfide	No	High	No	-2.03 (soluble)
14	Allyl methyl trisulfide	Yes	High	No	-1.43 (soluble)
15	Allixin	Yes	High	No	-3.89 (soluble)
16	Allicin	Yes	High	No	-1.7 (soluble)
17	Allyl methyl disulfide	Yes	High	No	-1.29 (soluble)
18	Ajoene	No	High	No	-2.32 (soluble)
19	Diallyl disulfide	Yes	High	No	-1.78 (soluble)
20	3-(Allylsulphinyl)-L-alanine	No	High	No	-0.21 (soluble)
21	3-Vinyl-1,2-dithiin	Yes	High	No	-0.93 (soluble)
22	Alliin	No	High	No	-0.21 (soluble)
23	Allyl prop-1-enyl disulfide	Yes	High	No	-1.41 (soluble)
24	Kaempferol	No	High	No	-3.82 (soluble)
25	Allyl mercaptan	Yes	High	No	-0.71 (soluble)

Screening of Physicochemical/Pharmacological Properties

The pharmacological properties of ligands such as lipophilicity (XlogP), Topological Polar Surface Area (TPSA), fraction Sp^3 hybridization, rotatable bonds, and molar refractivity (Table 2) were analyzed by the SwissADME (Table 9). The ligands met most of the range limits of physicochemical properties. The TPSA of quercetin (131.36) was slightly above the range limit of 20-130. Octadecane obeyed all the parameters except that of having 15 rotatable bonds instead of less than 9. Fraction Csp^3 of 1-Ethylquinolinium iodide, eugenol, and quercetin were slightly below the optimal value of 0.25. Still, the compounds were taken for further analysis because of their well-known anti-cancerous effects. The molar refractivity of a ligand responsible for good absorption and oral bioavailability was less than the optimal range for phenylacetic acid, diallyl sulfide, dimethyl disulfide, dimethyl trisulfide, allyl methyl disulfide, and allyl mercaptan.

Table 8. Lipinski filter analysis data of *Allium sativum* ligands from SwissADME.

S.N.	Ligand	Formula	Molecular weight	M Log P	Hydrogen acceptors	Hydrogen donors	Lipinski violations
1	1-Propenyl allyl thiosulfinate	$C_6H_{10}O_2S_2$	178.27	1.07	2	0	0
2	Carvacrol	$C_{10}H_{14}O$	150.22	2.76	1	1	0
3	Octadecane	$C_{18}H_{38}$	254.49	6.92	0	0	1
4	Allyl propyl disulfide	$C_6H_{12}S_2$	148.29	2.46	0	0	0
5	Phenylacetic acid	$C_8H_8O_2$	136.15	1.66	2	1	0
6	1-Ethylquinolinium iodide	$C_{11}H_{12}IN$	285.12	2.99	0	0	0
7	Diallyl sulfide	$C_6H_{10}S$	114.21	2.35	0	0	0
8	Dimethyl disulfide	$C_2H_6S_2$	94.2	0.84	0	0	0
9	Eugenol	$C_{10}H_{12}O_2$	164.2	2.01	2	1	0
10	Quercetin	$C_{15}H_{10}O_7$	302.24	-0.56	7	5	0
11	Diallyl trisulfide	$C_6H_{10}S_3$	178.34	2.35	0	0	0
12	Dimethyl trisulfide	$C_2H_6S_3$	126.26	0.84	0	0	0
13	Diallyl tetrasulfide	$C_6H_{10}S_4$	210.4	2.35	0	0	0
14	Allyl methyl trisulfide	$C_4H_8S_3$	152.3	1.67	0	0	0
15	Allixin	$C_{12}H_{18}O_4$	226.27	0.46	4	1	0

16	Allicin	$C_6H_{10}OS_2$	162.27	1.18	1	0	0
17	Allyl methyl disulfide	$C_4H_8S_2$	120.24	1.67	0	0	0
18	Ajoene	$C_9H_{14}OS_3$	234.4	2.1	1	0	0
19	Diallyl disulfide	$C_6H_{10}S_2$	146.27	2.35	0	0	0
20	3-(Allylsulphinyl)-L-alanine	$C_6H_{11}NO_3S$	177.22	-2.88	4	2	0
21	3-Vinyl-1,2-dithiin	$C_6H_8S_2$	144.26	1.96	0	0	0
22	Alliin	$C_6H_{11}NO_3S$	177.22	-2.88	4	2	0
23	Allyl prop-1-enyl disulfide	$C_6H_{10}S_2$	146.27	2.35	0	0	0
24	Kaempferol	$C_{15}H_{10}O_6$	286.24	-0.03	6	4	0
25	Allyl mercaptan	C_3H_6S	74.14	1.22	0	0	0

Table 9. Physicochemical properties of *Allium sativum* ligands obtained using SwissADME.

S.N.	Ligand	Fraction Csp3 SwissADME ref	Rotatable bonds	Topological polar surface area (TPSA)	Lipophilicity	Molecular refractivity (MR)
1	1-Propenyl allyl thiosulfinate	0.33	5	70.81	1.7	46.96
2	Carvacrol	0.4	1	20.23	3.49	48.01
3	Octadecane	1	15	0	9.37	88.64
4	Allyl propyl disulfide	0.67	5	50.6	2.45	45.66
5	Phenylacetic acid	0.12	2	37.3	1.41	37.99
6	1-Ethylquinolinium iodide	0.18	1	3.88	-2.87	66.37
7	Diallyl sulfide	0.33	4	25.3	2.16	37.6
8	Dimethyl disulfide	1	1	50.6	1.77	26.91
9	Eugenol	0.2	3	29.46	2.27	49.06
10	Quercetin	0	1	131.36	1.54	78.03
11	Diallyl trisulfide	0.33	6	75.9	2.64	52.78
12	Dimethyl trisulfide	1	2	75.9	1.35	34.5
13	Diallyl tetrasulfide	0.33	7	101.2	3.08	60.37
14	Allyl methyl trisulfide	0.5	4	75.9	1.99	43.64
15	Allixin	0.58	5	59.67	2.78	62.65
16	Allicin	0.33	5	61.58	1.31	45.88
17	Allyl methyl disulfide	0.5	3	50.6	1.55	36.05
18	Ajoene	0.33	8	86.88	1.71	67.41
19	Diallyl disulfide	0.33	5	50.6	2.2	45.19
20	3-(Allylsulphinyl)-L-alanine	0.5	5	99.6	-3.53	43.24
21	3-Vinyl-1,2-dithiin	0.33	1	50.6	2.05	43.08
22	Alliin	0.5	5	99.6	-3.53	43.24
23	Allyl prop-1-enyl disulfide	0.33	4	50.6	2.28	45.19
24	Kaempferol	0	1	111.13	1.9	76.01
25	Allyl mercaptan	0.33	1	38.8	1.16	23.99

Prediction of Ligand Toxicity

The ligands were subjected to toxicity assessment to enhance their safety profile and functional drug nature efficacy by the ADMET 2.0 web server. The tool assesses the rat oral acute toxicity based on toxicity categorization along with an empirical decision based on the LD50 (mg/kg) range limits as depicted in Table 10.

Aggregation Characteristics

The aggregation properties of ligands are analyzed by the Chem AGG (*https://admet.scbdd.com/ChemAGG/index/*) tool, where the drugs are classified into aggregators indicated by score 1 and non-aggregator denoted by score 0 along with probability scores. All 25 ligands taken for analysis fall into the non-aggregator class with a score of 0 and are likely to be potential lead molecules (Table 11).

The non-aggregator-type molecules do not interfere with other molecules easily, hence making them easy to synthesize into drug-active compounds. Such a property is defined by a synthetic accessibility (SA) parameter ranging from 0 to 10 score (easy to difficult) to be synthesized as a functional therapeutic molecule [22]. Bioavailability is calculated according to the ligand's ability to contribute to 10% of rat oral bioavailability through its polar surface area [40]. In Table 10, the bioavailability of 0.55 is good, while the allyl mercaptan, phenylacetic acid, and carvacrol drugs with a score value range of 1 are very easy to prepare according to SwissADME prediction. All the ligands are easy to process with a SA score below the 5-threshold range, thus likely to be drug candidates.

Table 10. Toxicity profile of *Allium sativum* ligands obtained using ADMET 2.0.

S. N	Ligands	Predicted LD50/rat oral acute toxicity	Toxicity category/level	Empirical decision
1	1-Propenyl allyl thiosulfinate	0/nil	Low	Excellent/non-toxic
2	Carvacrol	0/nil	Low	Excellent/non-toxic
3	Octadecane	0/nil	Low	Excellent/non-toxic
4	Allyl propyl disulfide	0/nil	Low	Excellent/non-toxic
5	Phenylacetic acid	0/nil	Low	Excellent/non-toxic
6	1-Ethylquinolinium iodide	0/nil	Low	Excellent/non-toxic
7	Diallyl sulfide	0/nil	Low	Excellent/non-toxic
8	Dimethyl disulfide	0/nil	Low	Excellent/non-toxic
9	Eugenol	0/nil	Low	Excellent/non-toxic
10	Quercetin	0/nil	Low	Excellent/non-toxic
11	Diallyl trisulfide	0/nil	Low	Excellent/non-toxic
12	Dimethyl trisulfide	0/nil	Low	Excellent/non-toxic
13	Diallyl tetrasulfide	0/nil	Low	Excellent/non-toxic
14	Allyl methyl trisulfide	0/nil	Low	Excellent/non-toxic
15	Allixin	0/nil	Low	Excellent/non-toxic
16	Allicin	0/nil	Low	Excellent/non-toxic
17	Allyl methyl disulfide	0/nil	Low	Excellent/non-toxic
18	Ajoene	0/nil	Low	Excellent/non-toxic
19	Diallyl disulfide	0/nil	Low	Excellent/non-toxic
20	3-(Allylsulphinyl)-L-alanine	0/nil	Low	Excellent/non-toxic
21	3-Vinyl-1,2-dithiin	0/nil	Low	Excellent/non-toxic
22	Alliin	0/nil	Low	Excellent/non-toxic
23	Allyl prop-1-enyl disulfide	0/nil	Low	Excellent/non-toxic
24	Kaempferol	0/nil	Low	Excellent/non-toxic
25	Allyl mercaptan	0/nil	Low	Excellent/non-toxic

Table 11. Aggregation properties of *Allium sativum* ligands obtained from Chem AGG.

S.N.	Ligand	Aggregator class	Bioavailability score	Synthetic accesibility SA score	Probability score
1	1-Propenyl allyl thiosulfinate	0	0.55	4.05	0.044
2	Carvacrol	0	0.55	1	0.073
3	Octadecane	0	0.55	2.49	0.024
4	Allyl propyl disulfide	0	0.55	2.95	0.076
5	Phenylacetic acid	0	0.85	1	0.013
6	1-Ethylquinolinium iodide	0	0.55	1.13	0.039
7	Diallyl sulfide	0	0.55	2.34	0.055
8	Dimethyl disulfide	0	0.55	2.33	0.04
9	Eugenol	0	0.55	1.58	0.044
10	Quercetin	0	0.55	3.23	0.067
11	Diallyl trisulfide	0	0.55	3.58	0.041
12	Dimethyl trisulfide	0	0.55	3.64	0.039
13	Diallyl tetrasulfide	0	0.55	3.63	0.055
14	Allyl methyl trisulfide	0	0.55	3.32	0.052
15	Allixin	0	0.55	3.12	0.088
16	Allicin	0	0.55	3.6	0.096
17	Allyl methyl disulfide	0	0.55	2.73	0.056
18	Ajoene	0	0.55	4.33	0.054
19	Diallyl disulfide	0	0.55	3.12	0.051
20	3-(Allylsulphinyl)-L-alanine	0	0.55	3.21	0.015
21	3-Vinyl-1,2-dithiin	0	0.55	4.27	0.027
22	Alliin	0	0.55	3.21	0.015
23	Allyl prop-1-enyl disulfide	0	0.55	3.84	0.113
24	Kaempferol	0	0.55	3.14	0.048
25	Allyl mercaptan	0	0.55	1.76	0.047

Boiled Egg Prediction

The Boiled egg is a pictorial representation of the permeation of ligands into BBB, GI tract, and P-glycoprotein (PGP) receptor as predicted by SwissADME. Figure 9 shows drug ligands such as Carvacrol and Eugenol present in the egg's yolk (yellow region) indicating both have high BBB permeation and GI absorption (HIA as in the legend). Kaempferol and Quercetin have high GI tract absorption only. 1-Ethylquinolinium iodide is non-permeated into BBB nor does have GI absorption. PGP+ indicates the ability of the ligand to be a substrate for the PGP efflux transporter protein which helps in drug/ligand excretion from the central nervous system/BBB. PGP indicates the ligand cannot be eliminated from the central nervous system by the PGP efflux transporter protein. As shown in Figure 9, none of the ligands are PGP substrates since the ligands are all indicated in red dots. Since the ligands are not intended to be transported across BBB, the PGP- parameter does not affect the ability of ligands to serve as anti-cancer agents. Ligands such as carvacrol, eugenol, kaempferol, quercetin, and 1-Ethylquinolinium iodide are chosen for boiled egg analysis for their best binding affinity scores to the target protein Bcl-2.

Macromolecular Structural Analysis

Bcl-2 protein is an apoptosis regulator. Their family of proteins acts as either initiators or inhibitors of programmed cell death mediated through energy-dependent biochemical mechanisms of mitochondria. Bcl-2 protein is an efficient therapeutic target for promoting tumor cell apoptosis in ALL. Hence, Bcl-2 (PDB ID 4AQ3) has 169 amino acid residues on A, B, C, D, E, and F chains as shown in Table 12, and is chosen as the target macromolecule for molecular docking. Prankweb server (*https://prankweb.cz/*) is a popular ligand binding site prediction server [41]. According to this tool, the

target macromolecule has 28 active sites in all the 6 chains of protein. The pocket 1 has 15 amino acid residues on E_105, E_108, E_112, E_63, E_67, E_70, E_71, E_74, E_77, E_91, E_92, E_95, E_96, F_82, F_83. Pocket 2 has 11 amino acid residues at B_104, B_105, B_108, B_112, B_63, B_67, B_70, B_71, B_74, B_92, B_96. Pocket 3 has 18 residues at A_104, A_105, A_108, A_112, A_63, A_67, A_70, A_71, A_74, A_77, A_91, A_92, A_95, A_96, C_82, C_83, E_162, E_58. Pocket 4 has 14 amino acid residues at B_160, B_162, B_58, D_104, D_105, D_108, D_112, D_63, D_67, D_70, D_71, D_74, D_92, D_96. Pocket 5 has 11 amino acid residues at F_104, F_105, F_108, F_112, F_63, F_67, F_70, F_71, F_74, F_92, F_96. Pocket 6 has 11 amino acid residues at C_104, C_105, C_108, C_112, C_63, C_67, C_70, C_71, C_74, C_92, C_96. Pocket 7 has 17 amino acid residues at A_160, A_161, A_162, A_58, A_62, E_103, E_104, E_105, E_107, E_157, E_160, E_161, E_59, E_62, E_63, E_66, E_67. Pocket 8 has 15 amino acid residues at B_103, B_104, B_107, B_157, B_160, B_161, B_59, B_62, B_63, B_67, D_160, D_161, D_162, D_58, D_62. Pocket 9 has 11 amino acid residues at B_103, B_151, B_156, B_159, B_160, D_103, D_147, D_151, D_156, D_159, D_160. Pocket 10 has 20 amino acid residues A_142, A_143, A_145, A_146, A_149, A_150, D_111, D_114, D_115, D_118, D_119, D_122, D_22, D_25, D_26, D_64, D_68, D_71, D_72, D_75. Pocket 11 has 11 amino acids at sites B_68, B_72, B_76, E_100, E_101, E_143, E_146, E_147, E_150, E_151, E_97. Pocket 12 has 13 residues at B_160, B_161, B_58, B_62, D_104, D_107, D_157, D_161, D_59, D_62, D_63, D_66, D_67. Pocket 13 has 13 amino acid residues at B_111, B_115 B_118, B_22, B_25, B_26, B_64, B_68, B_71, B_72, B_75, E_146, E_150. Pocket 14 has 13 residues at A_102, A_104, A_105, A_107, A_59, A_63, A_66, A_67, E_160, E_161, E_162, E_58, E_62. Pocket 15 has 10 amino acids from A_103, A_151, A_156, A_159, A_160, E_103, E_151, E_156, E_159, E_160. Pocket 16 has 9 residues at F_135, F_138, F_139, F_142, F_143, F_86, F_89, F_90, F_94. Pocket 17 has 10 amino acids sites at A_100, A_101, A_143, A_146, A_147, A_150, A_151, D_68, D_69, D_72. Pocket 18 has 10 residues at A_103, A_104, A_107, A_157, A_160, A_161, A_59, A_63, E_160, E_161. Pocket 19 has 11 amino acid residues at A_158, A_159, A_160, A_162, E_102, E_104, E_105, E_108, E_63, E_96, E_99. Pocket 20 has 10 residues at C_111, C_114, C_115, C_118, C_22, C_26, C_64, C_68, C_71, C_75. Pocket 21 has 9 amino acid sites at D_135, D_138, D_139, D_143, D_86, D_89, D_90, D_93, D_94. Pocket 22 has 10 residues at E_111, E_115, E_118, E_22, E_26, E_64, E_68, E_71, E_72, E_75. Pocket 23 has 6 residues at B_135, B_138, B_139, B_143, B_89, B_90. Pocket 24 has 8 amino acid residues at C_103, C_104, C_107, C_157, C_160, C_161, C_59, C_63. Pocket 25 has 7 residues at F_103, F_104, F_107, F_157, F_161, F_59, F_63. Pocket 26 has 6 residues at C_135, C_138, C_139, C_143, C_89, C_90. Pocket 27 has 6 residues at F_111 F_114 F_115 F_118 F_22 F_26 F_64 F_68 F_71 F_75. Pocket 28 has 10 amino acid residues at A_135 A_138 A_139 A_143 A_86 A_89 A_90 A_93. Similar mutagenesis has been encountered in all the A, B, C, D, E, and F chains of Bcl-2 protein since they are identical. The mutagenesis site prediction was carried out by the computed atlas of surface topography of proteins (CASTp) (*http://sts.bioe.uic.edu/castp/index.html?2pk9*) [42].

In the A chain, mutagenesis at 97–100th, 103, 104, 105, 147, 149, 150, 151, 153 to 156, and 159th residues leads to loss of BAX binding and subsequent loss of anti-apoptotic activity. There was no effect on NLRP1-induced IL1B release nor homodimerization observed in CASTp mutagenesis analysis.

Molecular Docking

PyRx Autodock Vina software was used to perform molecular docking. 25 ligands of *A. sativum* were docked with chains A, B, C, D, and E, and F, of the Bcl-2 target to obtain a holistic and comprehensive understanding of protein-ligand interactions. From this, 5 best ligands namely kaempferol, quercetin, 1-Ethylquinolinium iodide, carvacrol, and eugenol with binding affinities above -7 formed from target protein-ligand complex were chosen. Ligands with their corresponding binding affinities are displayed in Table 13.

Visualization of Target Protein-Ligand Complexes

Followed by docking, the target protein-ligand complex can be visualized by the Discovery Studio v24.1.0.23298 (BIOVIA) tool. The 3D interactions of target Bcl-2 with kaempferol, quercetin, 1-Ethylquinolinium iodide, carvacrol, and eugenol are shown in Figures 10(a) and (b), Figure 11(a), and

(b), and Figure 12. 2D interactions were facilitated by different types of bonds such as the conventional hydrogen bond, carbon-hydrogen bond, pi-donor hydrogen bond, pi-sigma, pi-pi stacked, pi-alkyl, alkyl, van der Waals forces, and other unfavorable donor-donor interactions between the amino acid residues of the target protein and the selected ligands kaempferol, quercetin, 1-ethyl quinolinium iodide, carvacrol, and eugenol as depicted in the Figures 13(a) and (b), Figure 14(a) and (b), and Figure 15. The other significant details of 2D interactions including the ligand-protein distance, type, and category of bonds are listed in Tables 14 to 18.

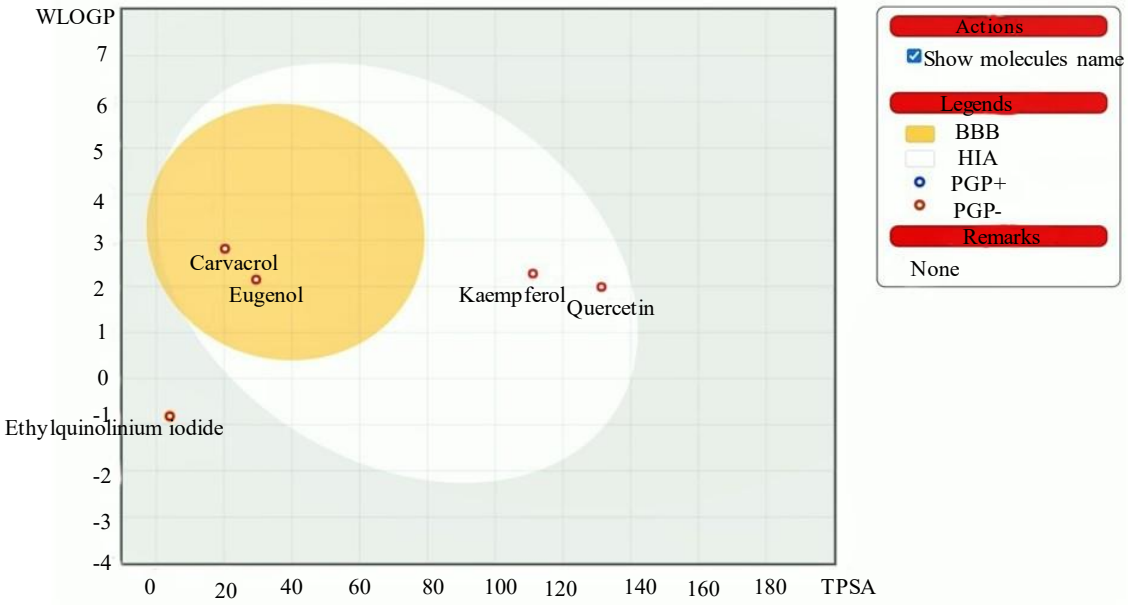

Figure 9. Boiled egg representation of ligands for ADME analysis.

Table 12. Details of macromolecule 4AQ3 from RCSB PDB

Molecule	Chains	Sequence length	Organism	Details
Apoptosis regulator Bcl-2, Bcl-2-like protein 1	A, B, C, D, E, and F	169	*Homo sapiens*	Mutations: 2

Table 13. Binding affinities of A, B, C, D, E, and F chains of target protein with *A. sativum* ligands obtained from PyRx.

S. N.	Ligands	Binding affinity (Kcal/mol)
1	1-Ethylquinolinium iodide	-7.7
2	1-Propenyl allyl thiosulfinate	-4.1
3	3-(Allylsulphinyl)-L-alanine	-5.1
4	3-Vinyl-1,2-dithiin	-5.2
5	Ajoene	-4.2
6	Allicin	-4.2
7	Alliin	-5.3
8	Allixin	-6
9	Allyl mercaptan	-2.8
10	Allyl methyl disulfide	-3.6
11	Allyl methyl trisulfide	-3.7
12	Allyl prop-1-enyl disulfide	-3.7
13	Allyl propyl disulfide	-3.7
14	Carvacrol	-7.5
15	Diallyl disulfide	-3.5
16	Diallyl sulfide	-4.3
17	Diallyl tetrasulfide	-3.5

18	Diallyl trisulfide	-3.7
19	Dimethyl disulfide	-2.4
20	Dimethyl trisulfide	-2.8
21	Eugenol	-7.3
22	Kaempferol	-7.9
23	Octadecane	-4.9
24	Phenylacetic acid	-7.1
25	Quercetin	-7.7

Visualization of the 3D and 2D docking of Bcl-2 with Kaempferol

As per Tables 13 and 14, the ligand kaempferol interacts with amino acids ASP D:61, ARG D:65, GLN D:25, ARG D:68, ASP A:150, THR A:146, ARG D:26, and ARG B:66 of Bcl-2 target protein. The binding affinity of the ligand to target Bcl-2 is -7.9.

Visualization of the 3D and 2D docking of Bcl-2 with Quercetin

From Tables 13 and 15, the ligand Quercetin has strong 3D interactions with the Bcl-2 protein with a binding affinity of -7.7. The 2D interaction sites of ligands with target BCL-2 protein include ARG B:66, ASP A:150, ASP D:61, ARG D:65, ARG D:68, SER D:64, and GLN D:25.

Visualization of the 3d and 2d Docking of Bcl-2 With 1-Ethylquinolinium Iodide

The 3D binding interaction score of 1-Ethylquinolinium iodide with Bcl-2 protein is -7.7. Amino acids, such as PHE B:63, VAL B:107, ALA B:59, TYR B:67, ARG B: 66, TYR D:161, and TYR B:67 of Bcl-2 protein were involved in binding with ligand 1-Ethylquinolinium iodide as shown in the 3D and 2D interactions displayed in (Tables 13 and 16).

Visualization of the 3D and 2D docking of Bcl-2 with Carvacrol

Tables 13 and 17 show the 2D interactions at amino acid residues TYR A:161, VAL E:107, and ALA E:59 of protein Bcl-2 and ligand carvacrol. Their binding affinity from 3D docking is found to be -7.5.

Visualization of the 3D And 2D Docking of Bcl-2 With Eugenol

The 3D binding interactions between Bcl-2 and ligand eugenol are found to be -7.3, while the Bcl-2 amino acids, such as GLU D:58, ASP D:62, TYR B:67, TYR D: 161, PHE B:63, PHE B:157, VAL B:107, and LEU B:160, interact with ligand eugenol, as shown in (Tables 13 and 18).

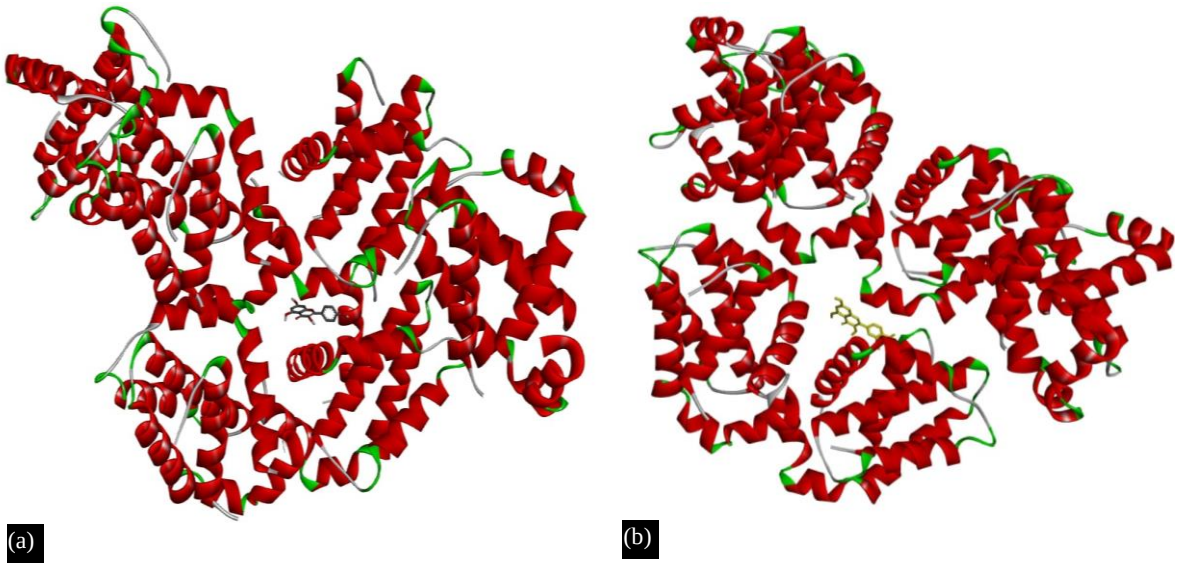

Figure 10. 3D interactions of target protein Bcl-2 with (a) Kaempferol (ligand indicated in black), and (b) Quercetin (ligand indicated in yellow).

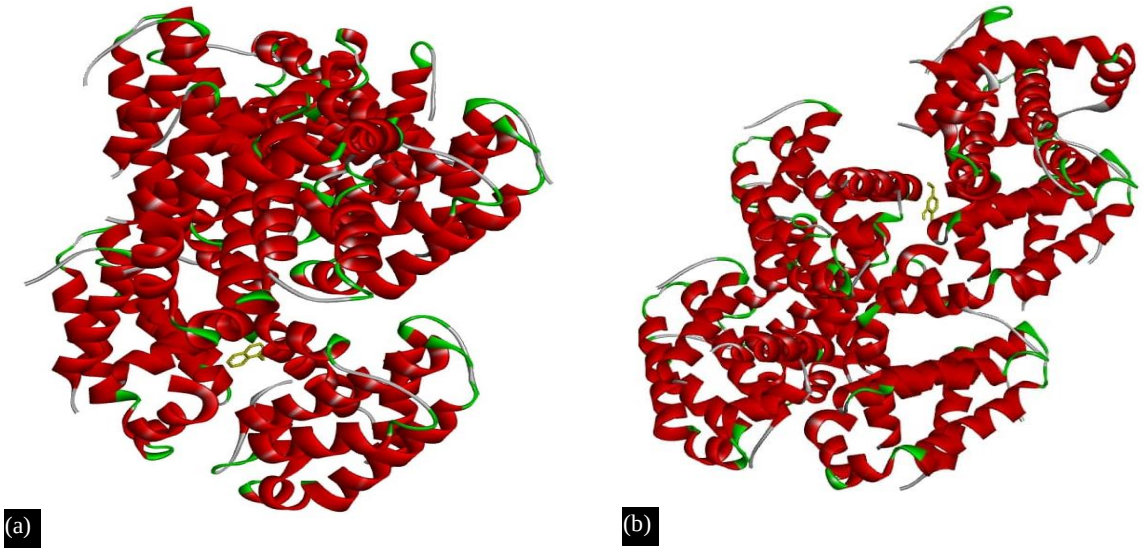

Figure 11. 3D interactions of target protein Bcl-2 with (a) 1-Ethylquinolinium iodide (ligand indicated in yellow), and (b) Carvacrol (ligand indicated in yellow).

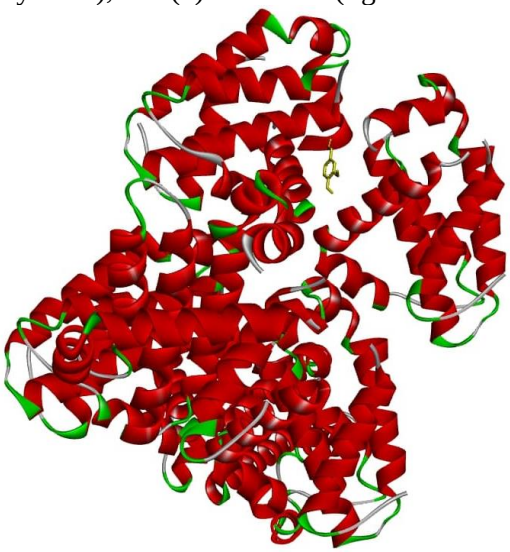

Figure 12. 3D interactions of target protein Bcl-2 with eugenol (ligand indicated in yellow).

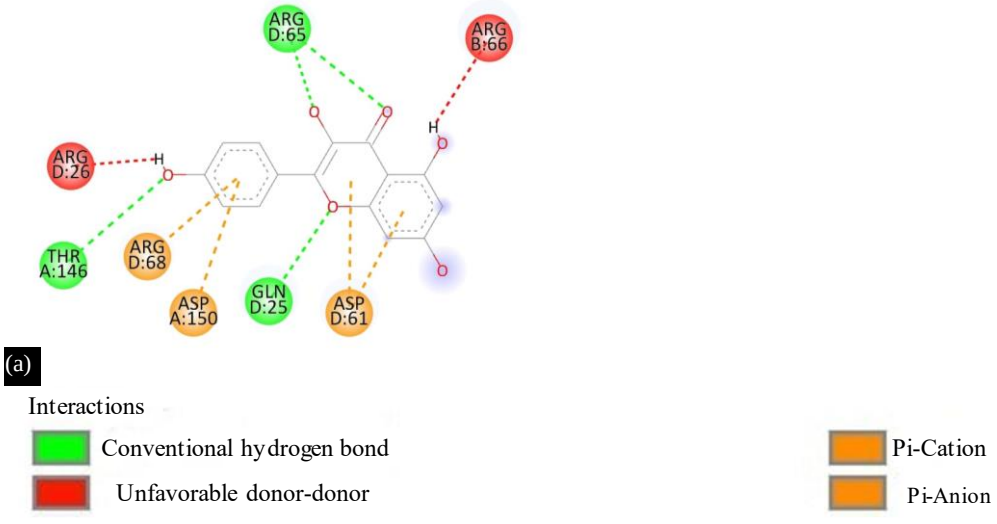

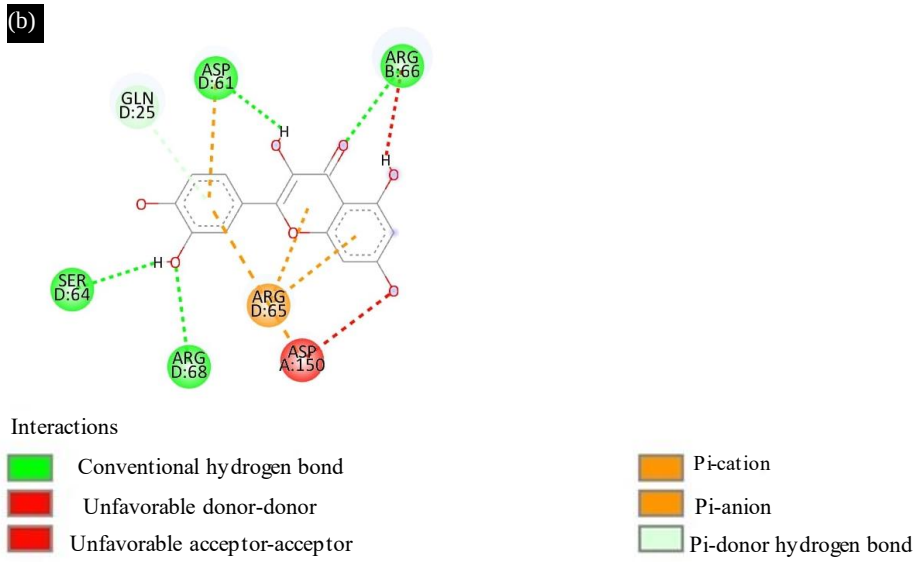

Figure 13. 2D interactions between Bcl-2 and (A) Kaempferol (B) Quercetin.

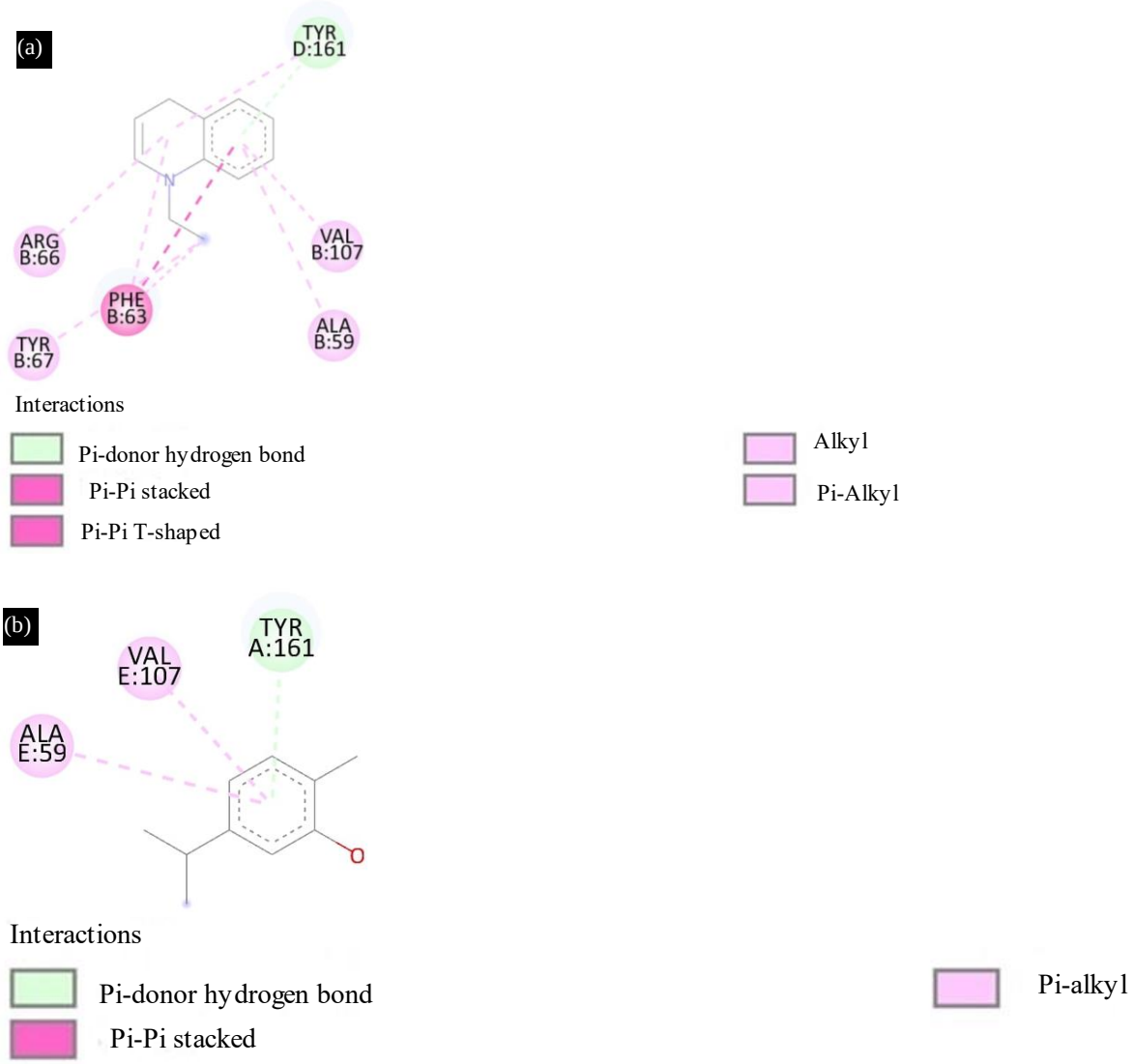

Figure 14. 2D interactions between Bcl-2 and (a) 1-Ethylquinolinium iodide, (b) Carvacrol.

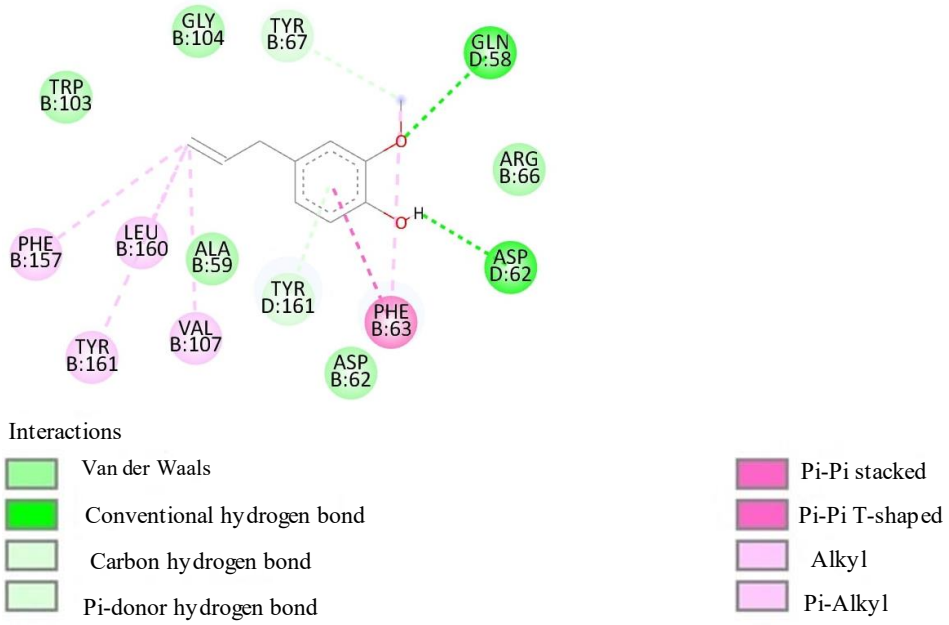

Figure 15. 2D interactions between Bcl-2 and Eugenol.

Table 14. 2D docking between Bcl-2 with Kaempferol.

Amino acid site/position	Distance	Bond classification	Type of bond
ASP D:61	3.79	Hydrophobic	Pi-cation/Pi-anion
ASP D:61	3.97	Hydrophobic	Pi-cation/Pi-anion
ARG D: 65	2.80	Hydrogen	Conventional hydrogen bond
ARG D:65	3.27	Hydrogen	Conventional hydrogen bond
GLN D:25	2.95	Hydrogen	Conventional hydrogen bond
ARG D:68	3.50	Hydrophobic	Pi-cation/Pi-anion
Amino acid site/position	Distance	Bond classification	Type of bond
ASP A:150	4.79	Hydrophobic	Pi-cation/Pi-anion
THR A:146	2.97	Hydrogen	Conventional hydrogen bond
ARG D:26	2.07		Unfavorable donor-donor interaction
ARG B:66	2.59		Unfavorable donor-donor interaction

Table 15. 2D docking between Bcl-2 with Quercetin.

Amino acid site/position	Distance	Bond classification	Type of bond
ARG B:66	2.94	Hydrogen	Conventional hydrogen bond/Pi-donor hydrogen bond
ARG B:66	2.43		Unfavorable donor-donor/unfavorable acceptor-acceptor interactions
ASP A:150	3.00		Unfavorable donor-donor/unfavorable acceptor-acceptor interactions
ASP D:61	2.20	Hydrogen	Conventional hydrogen bond/Pi-donor hydrogen bond
ASP D:61	4.44	Hydrophobic	Pi-cation/Pi-anion
ARG D:65	4.81	Hydrophobic	Pi-cation/Pi-anion
ARG D: 65	3.94	Hydrophobic	Pi-cation/Pi-anion
Amino acid site/position	Distance	Bond classification	Type of bond
ARG D: 65	3.56	Hydrophobic	Pi-cation/Pi-anion
ARG D:68	3.26	Hydrogen	Conventional hydrogen bond
SER D:64	3.12	Hydrogen	Conventional hydrogen bond
GLN D:25	3.57	Hydrogen	Pi-donor hydrogen bond

Table 16. 2D docking between Bcl-2 with 1-Ethylquinolinium iodide.

Amino acid site/position	Distance	Bond classification	Type of bond
PHE B:63	***5.65***	***Hydrophobic***	***Pi-Pi stacked/Pi-Pi T-shaped bond***
VAL B:107	5.18	Hydrophobic	Alkyl/Pi-alkyl
ALA B:59	4.77	Hydrophobic	Alkyl/Pi-alkyl
TYR B:67	4.85	Hydrophobic	Alkyl/Pi-alkyl
ARG B:66	5.05	Hydrophobic	Alkyl/Pi-alkyl
PHE B:63	5.44	Hydrophobic	Alkyl/Pi-alkyl
TYR D:161	4.18	Hydrogen	Pi-donor hydrogen bond
PHE B:63	4.20	Hydrophobic	Pi-Pi stacked/Pi-Pi T-shaped
TYR B:67	4.26	Hydrophobic	Alkyl/Pi-alkyl

Table 17. 2D docking between Bcl-2 with carvacrol.

Amino acid site/position	Distance	Bond classification	Type of bond
TYR A:161	3.83	Hydrogen	Pi-donor hydrogen bond
VAL E:107	4.27	Hydrophobic	Pi-Pi stacked
Amino acid site/position	Distance	Bond classification	Type of bond
ALA E:59	5.18 & 4.99	Hydrophobic	Pi-alkyl

Table 18. 2D docking between Bcl-2 with eugenol.

Amino acid site/position	Distance	Bond classification	Type of bond
GLN D:58	3.15	Hydrogen	Conventional hydrogen bond
ASP D:62	2.34	Hydrogen	Conventional hydrogen bond
TYR B:67	3.68	Hydrogen	Carbon-hydrogen bond/Pi-donor hydrogen bond
TYR D:161	3.73	Hydrogen	Carbon-hydrogen bond/Pi-donor hydrogen bond
PHE B:63	4.89	Hydrophobic	Alkyl/Pi-alkyl
PHE B:157	4.69	Hydrophobic	Alkyl/Pi-alkyl
LEU B:160	4.87	Hydrophobic	Alkyl/Pi-alkyl
VAL B:107	5.32	Hydrophobic	Alkyl/Pi-alkyl
TYR B:161	5.21	Hydrophobic	Alkyl/Pi-alkyl
PHE B:63	5.50	Hydrophobic	Alkyl/Pi-alkyl

DISCUSSION

Garlic (*Allium sativum*) is the second most commonly used member of the *Amaryllidaceae* family after onion (*Allium cepa*) and is used as an additive, spice, and medicinal plant worldwide. The chemical constituents of garlic namely the organosulfur group of compounds offer diverse biological activities and health benefits [43]. Other significant groups of compounds seen in garlic include flavonoids, terpenoids, saponins, peptides, steroids, and phenols [44]. The multiple medicinal properties of garlic with a low toxicity profile is what makes garlic an attractive choice for drug discovery [45]. Some of the well-studied biological activities of garlic include anti-cancer, anti-diabetic, anti-hypertensive, reno-protective, anti-atherosclerotic, antimicrobial, and antioxidant [46]. Early studies reported that organosulfur compounds such as allicin, diallyl disulfide, alliin, diallyl sulfide, allyl mercaptan, and S-allyl cysteine have anti-cancer properties [47, 48]. Kaempferol, a flavonoid is reported to increase the levels of pro-apoptotic enzymes and proteins, such as cleaved caspase-9, -7, -3, p21, p53, Bax, and Poly (ADP-ribose) polymerases [49] and decreased the levels of anti-apoptotic proteins Bcl2 and polo-like kinase 1 (PLK-1) [50]. The Kaempferol has passed all the Lipinski rules when docked against breast cancer biomarkers estrogen receptor, progesterone receptor, androgen receptor, and glucocorticoid receptor [51]. As a Bcl-2 inhibitor, kaempferol's docking score was in the range of -6.00 to -3.78 kcal/mol provided by the glide-ligand docking tool of Schrödinger Maestro 12.5 compared to the other

co-crystallized ligand with a score of -3.62 kcal/mol [52]. Quercetin is a phytoflavonol known to exhibit anti-cancer and anti-inflammatory activities. The flavonol content in the genus *Allium* differs widely depending on the growing conditions and storage. From animal studies, it is revealed that quercetin elevated the antioxidant levels in the plasma. One of the quercetin glucosides namely quercetin-4'-O-glucoside has high anti-proliferative effect in the HepG2 liver carcinoma cells [53]. Quercetin promotes cell death in prostate cancer through apoptosis and necrosis by disturbing the mitochondrial homeostasis and increasing the reactive oxygen species (ROS) levels by oxidative stress [54]. Quercetin studied to exert apoptotic activities against different cancer lines such as leukemia HL-60 [55]. Quercetin has cleared all the Lipinski parameters and also has good plasma protein binding efficiency during molecular docking with breast cancer receptors [56]. The NK-4 (4,4'-[3-{2-(1-ethyl-4(1H)-quinolylidene) ethylidene}pro-penylene] bis (1-ethyl quinolinium iodide)) (lumin) has biological effects on antimicrobial, macrophage-activating, anti-cancer properties. They are found to promote anti-apoptotic activities in neuronal cells [57]. Carvacrol is a monoterpenoid phenol with biological effects, including antimicrobial, insecticidal, anti-angiogenic, and anti-tumor activity. The carvacrol nanoemulsion mediated ROS formation in the lung cancer A549, activated the significant regulators of apoptosis such as p-JNK, Bax, and Bcl2 as well as the promoted the release of cytochrome C, along with initiation of caspase cascade. This suggests that the nano-formulated carvacrol leads to apoptosis in A549 cells through ROS and could be a promising candidate for lung cancer therapy [58]. The anti-cancer activity of carvacrol against malignant cells is manifested with downregulated expressions of matrix metalloprotease 2 and 9, initiating the apoptosis by increasing the expression of pro-apoptotic proteins, disruption of mitochondrial membrane, suppression of extracellular signal-regulated kinase 1/2 mitogen-activated protein kinase signal transduction, and also lowering of the phosphoinositide 3-kinase/protein kinase B. Antiproliferative effect of carvacrol is attributed to the hydroxyl group at its para-position as reported for its ability to inhibit the enzymes like ornithine decarboxylase, cyclooxygenase-2, lipoxygenase-5, and hyaluronidase responsible for carcinogenesis [59]. The cavacrol has a binding affinity score of -7.5 kcal/mol with the mammalian target of rapamycin (mTOR) receptor biomarker for breast cancer. Good oral absorption and bioavailability are also shown by this compound with no Lipinski rule violation [60, 61]. Eugenol is primarily derived from clove oil as a phenolic aromatic ingredient. Eugenol follows various anti-carcinogenesis mechanisms like promotion of apoptosis, cell cycle arrest, antiproliferation, inhibition of migration, angiogenesis, and metastasis on several cancer cell lines. Eugenol is also used as an adjuvant therapy along with chemotherapy in patients to reduce their therapeutic toxicity burden. When eugenol is subjected to oxidation and other biochemical reactions, its chemical stability is low and hence, oral bioavailability is poor. Hence, eugenol encapsulation is the preferred method of dosage administration to avoid early absorption and improve solubility, and the subsequent mechanism of action. In the promyelocytic leukemic cell line HL60, eugenol affected increased ROS and lowered the mitochondrial membrane potential leading to apoptosis stimulation [62, 63]. Some of the Eugenol derivatives synthesized as thymidylate synthase (TS) inhibitors in prostate cancer had passed all the Lipinski rules along with good bioavailability scores indicating their potential as orally active drug candidates [64].

CONCLUSION

This *in silico* analysis was carried out to determine the less toxic natural-based alternative to the chemotherapeutic Bcl-2 inhibitor drugs for ALL. Molecular docking of the apoptotic regulator Bcl-2 protein, an anti-apoptotic agent with flavonoids like kaempferol, quercetin, anti-cancer agent 1-Ethylquinolinium iodide, terpenoid carvacrol, and polyphenol eugenol showed strong binding affinity scores of above -7 than the average binding affinity range of -2 to -5 of the renowned anti-cancer organosulfur compounds of *Allium sativum.* Hence, the above secondary metabolites of garlic are found to be a better fit as Bcl-2 inhibitors than the organosulfur groups. However, more evident molecular pathway interactions *in vitro* and preclinical studies are required to prove the results of virtual screening.

Acknowledgment

I hereby acknowledge the Department of Bioinformatics, BioNome, Bengaluru, India, for providing computational facilities and support in the scientific research services. I thank Ms. Samiksha Bhor for her assistance throughout the project.

Conflict of Interest

The authors declare no conflict of interest.

Funding

This research received no external funding.

Abbreviations

ADME: Absorption, Distribution, Metabolism, and Excretion
ALL: Acute Lymphoblastic Leukemia
BAD: BCL2 Associated Agonist of Cell Death
BAK1: BCL2-Antagonist-Killer 1
B-ALL: B-Cell Acute Lymphoblastic Leukemia
Bax: Bcl-2-Associated X-Protein
BBB: Blood Brain Barrier
Bcl-2: B-Cell Leukemia 2
BCL2L1: Bcl-2-Like Protein 1
BCL2L11: Bcl-2-Like 11 Protein
Bcl-XL: Bcl-Extra Large
BCP-ALL: B-Cell Precursor Acute Lymphoblastic Leukemia
BECN1: Beclin 1
BH3: Bcl-2 Homology 3
BIK: BCL2 Interacting Killer
BIM: Bcl-2 Interacting Mediator of cell death
BIOVIA: Protein Visualizer Discovery Studio v24.1.0.23298
BNIP3: Bcl-2 Nineteen Kilodalton Interacting Protein
Canonical SMILES: Canonical Simplified Molecular Input Line Entry Specification
CASTp: Computed Atlas of Surface Topography of Proteins
CCRF-CEM: Human Caucasian Acute Lymphoblastic Leukemia Cell Line
GI: Gastrointestinal
IMPPAT: Indian Medicinal Plants, Phytochemistry and Therapeutics
PDBQT: Protein Data Bank, Partial Charge (Q), & Atom Type (T)
PD Bsum: Pictorial Database of 3D Structures in the Protein Data Bank
PGP: P-glycoprotein
PMAIP1: Phorbol-12-Myristate-13-Acetate-Induced Protein 1
RCSB PDB: Research Collaboratory for Structural Bioinformatics Protein Data Bank
RMSD LB: Root Mean Square Deviation Lower Boundary
RMSD UB: Root Mean Square Deviation Upper Boundary
SDF: Structured Data File
T-ALL: T-cell Acute Lymphoblastic Leukemia
TP53: Tumor Protein 53
TPSA: Topological Polar Surface Area

REFERENCES

1. Terwilliger T, Abdul-Hay M. Acute lymphoblastic leukemia: a comprehensive review and 2017 update. Blood Cancer J. 2007;7(6):e577–e577. doi:10.1038/bcj.2017.53.
2. Abiri B, Kelishadi R, Sadeghi H, Azizi-Soleiman F. Effects of maternal diet during pregnancy on the risk of childhood acute lymphoblastic leukemia: a systematic review. Nutrition and cancer. 2016 Oct 2;68(7):1065–72.
3. Blanco-Lopez J, Iguacel I, Pisanu S, Almeida C, Steliarova-Foucher E, Sierens C, Huybrechts I. Role of maternal diet in the risk of childhood acute leukemia: A systematic review and meta-analysis. Int J Environ Res Public Health. 2023;20(7):5428. doi:10.3390/ijerph20075428.

4. Ekpa QL, Akahara PC, Anderson AM, Adekoya OO, Ajayi OO, Alabi PO, Okobi OE, Jaiyeola O, Ekanem MS. A review of acute lymphocytic leukemia (ALL) in the pediatric population: Evaluating current trends and changes in guidelines in the past decade. Cureus. 2023;15(12):e49930. doi:10.7759/cureus.49930.
5. Huang FL, Yu SJ, Li CL. Role of autophagy and apoptosis in acute lymphoblastic leukemia. Cancer Control. 2021;28. doi:10.1177/10732748211019.
6. Olivas-Aguirre M, Pottosin I, Dobrovinskaya O. Mitochondria as emerging targets for therapies against T cell acute lymphoblastic leukemia. J Leukoc Biol. 2019;105(5):935–946. doi:10.1002/jlb.5vmr0818-330rr.
7. Hogarth LA, Hall AG. Increased BAX expression is associated with an increased risk of relapse in childhood acute lymphocytic leukemia. Blood. 1999:93(8):2671–2678. doi:10.1182/blood.V93.8.2671.
8. Moazami-Goudarzi M, Farshdousti-Hagh M, Hoseinpour-Feizi A, Talebi M, Movassaghpour-Akbari AA, Shams-Asanjan K, Eyvazi-Ziyaee J, Seifi M. The acute lymphoblastic leukemia prognostic scoring whether it is possible by BCL-2, BAX gene promoter genotyping. Caspian J Intern Med. 2016;7(2):105–113.
9. Ghasemi A, Khanzadeh T, Heydarabad ZM, Khorrami A, Esfahlan AJ, Ghavipanjeh S, et al. Evaluation of BAX and BCL-2 gene expression and apoptosis induction in acute lymphoblastic leukemia cell line CCRFCEM after high-dose prednisolone treatment. Asian Pac J Cancer Prev. 2018;19(8):2319–2323. doi:10.22034/APJCP.2018.19.8.2319.
10. Iacovelli S, Ricciardi MR, Allegretti M, Mirabilii S, Licchetta R, Bergamo P, et al. Co-targeting of Bcl-2 and mTOR pathway triggers synergistic apoptosis in BH3 mimetics resistant acute lymphoblastic leukemia. Oncotarget. 2015;6(31):32089–32103. doi:10.18632/oncotarget.5156.
11. Tsujimoto Y, Finger LR, Yunis J, Nowell PC, Croce CM. Cloning of the chromosome breakpoint of neoplastic B cells with the t (14;18) chromosome translocation. Sci. 1984;226(4678):1097–1099. doi:10.1126/science.60932.
12. Tsujimoto Y, Jaffe E, Cossman J, Gorham J, Nowell PC, Croce CM. Clustering of breakpoints on chromosome 11 in human B-cell neoplasms with the t (11;14) chromosome translocation. Nat. 1985;315(6017):340–343. doi:10.1038/315340a0.
13. Korsmeyer SJ, Shutter JR, Veis DJ, Merry DE, Oltvai ZN. Bcl-2/Bax: A rheostat that regulates an anti-oxidant pathway and cell death. Semin Cancer Biol. 1993;4(6):327–332.
14. Jabbour E, O'Brien S, Konopleva M, Kantarjian H. New insights into the pathophysiology and therapy of adult acute lymphoblastic leukemia. Cancer. 2015;121(15):2517–2528. doi:10.1002/cncr.29383.
15. Zhang Y, Liu X, Ruan J, Zhuang X, Zhang X, Li Z. Phytochemicals of garlic: Promising candidates for cancer therapy. Biomed Pharmacother. 2020;123:109730. doi:10.1016/j.biopha.2019.109730.
16. Szklarczyk D, Gable AL, Lyon D, Junge A, Wyder S, Huerta-Cepas J, Mering C. STRING v11: protein–protein association networks with increased coverage, supporting functional discovery in genome-wide experimental datasets. Nucleic Acids Res. 2019;47(D1):D607–D613. doi:10.1093/nar/gky1131.
17. Berman HM. The Protein Data Bank. Nucleic Acids Res. 2000;28(1):235–242. doi:10.1093/nar/28.1.235.
18. Zardecki C, Dutta S, Goodsell DS, Lowe R, Voigt M, Burley SK. PDB-101: Educational resources supporting molecular explorations through biology and medicine. Protein Sci. 2022;31(1):129–140. doi:10.1002/pro.4200.
19. Baroroh U, Biotek M, Muscifa ZS, Destiarani W, Rohmatullah FG, Yusuf M. Molecular interaction analysis and visualization of protein-ligand docking using Biovia Discovery Studio Visualizer. Indones J Comput Biol. 2023;2(1):22–30.
20. Mohanraj K, Karthikeyan BS, Vivek-Ananth RP, Chand RPB, Aparna SR, Mangalapandi P, Samal A. IMPPAT: A curated database of Indian medicinal plants, phytochemistry and therapeutics. Sci Rep. 2018;8:4329. doi:10.1038/s41598-018-22631-z.

21. Kim S, Chen J, Cheng T, Gindulyte A, He J, He S, Li Q, Shoemaker BA, Thiessen PA, Yu B, Zaslavsky L. PubChem in 2021: new data content and improved web interfaces. Nucleic Acids Res. 2021;49(D1):D1388–D1395. doi:10.1093/nar/gkaa971.
22. Daina A, Michielin O, Zoete V. SwissADME: a free web tool to evaluate pharmacokinetics, drug-likeness and medicinal chemistry friendliness of small molecules. Sci Rep. 2017;7(1):42717. doi:10.1038/srep42717.
23. Wang H, Irigoyen S, Liu J, Ramasamy M, Padilla C, Bedre R, Yang C, Thapa SP, Mulgaonkar N, Ancona V, He P, Coaker G, Fernando S, Mandadi KK. Inhibition of a conserved bacterial dual-specificity phosphatase confers plant tolerance to Candidatus liberibacter spp. iSci. 2024;27(3): 109232. doi:10.1016/j.isci.2024.109232.
24. Xiong G, Wu Z, Yi J, Fu L, Yang Z, Hsieh C, Yin M, Zeng X, Wu C, Lu A, Chen X, Hou T, Cao D. ADMETlab 2.0: an integrated online platform for accurate and comprehensive predictions of ADMET properties. Nucleic acids Res. 2021;49(W1):W5–W14. doi:10.1093/nar/gkab255.
25. Gadaleta D, Vuković K, Toma C, Lavado GJ, Karmaus AL, Mansouri K, Kleinstreuer NC, Benfenati E, Roncaglioni A. SAR and QSAR modeling of a large collection of LD50 rat acute oral toxicity data. J Cheminform. 2019;11(1):58. doi:10.1186/s13321-019-0383-2.
26. Kondapuram SK, Sarvagalla S, Coumar MS. Docking-Based Virtual Screening using PyRx Tool: Autophagy Target Vps34 as a Case Study. In: Coumar MS, editor. Molecular Docking for Computer-Aided Drug Design. United States: Academic Press; 2021. 463–477. doi:10.1016/C2019-0-04960-6.
27. Devaurs D, Antunes DA, Hall-Swan S, Mitchell N, Moll M, Lizée G, Kavraki LE. Using parallelized incremental meta-docking can solve the conformational sampling issue when docking large ligands to proteins. BMC Mol Cell Biol. 2019;20:1–5. doi:10.1186/s12860-019-0218-z.
28. Kelekar A, Chang BS, Harlan JE, Fesik SW, Thompson CB. Bad is a BH3 domain-containing protein that forms an inactivating dimer with Bcl-XL. Mol Cell Biol. 1997;17(12):7040–7046. doi:10.1128/MCB.17.12.7040.
29. Yang E, Zha J, Jockel J, Boise LH, Thompson CB, Korsmeyer SJ. Bad, a heterodimeric partner for Bcl-XL and Bcl-2, displaces bax and promotes cell death. Cell Press. 1995;80(2):285–291.
30. Strasser A. The role of BH3-only proteins in the immune system. Nat Rev Immunol. 2005;5(3):189–200. doi:10.1038/nri1568.
31. Lee AJ, Liao HJ, Hong JR. Overexpression of Bcl2 and Bcl2L1 can suppress Betanodavirus-induced type III cell death and autophagy induction in GF-1 cells. Symmetry. 2022;14(2):360. doi:10.3390/sym14020360.
32. Marquez RT, Xu L. Bcl-2: Beclin 1 complex: multiple, mechanisms regulating autophagy/apoptosis toggle switch. Am J Cancer Res. 2012;(2):214–221.
33. Burton TR, Gibson SB. The role of Bcl-2 family member BNIP3 in cell death and disease: NIPping at the heels of cell death. Cell Death Differ. 2009;16(4):515–523. doi:10.1038/cdd.2008.185.
34. Li X, Miao X, Wang H, Xu Z, Li B. The tissue dependent interactions between p53 and Bcl-2 in vivo. Oncotarget. 2015;6(34):35699–35709. doi:10.18632/oncotarget.5372.
35. Kanehisa M, Goto S. KEGG: kyoto encyclopedia of genes and genomes. Nucleic Acids Res. 2000;28(1):27–30. doi:10.1093/nar/28.1.27.
36. Laskowski RA, Jabłońska J, Pravda L, Vařeková RS, Thornton JM. PDBsum: Structural summaries of PDB entries. Protein Sci. 2018;27(1):129–134. doi:10.1002/pro.3289.
37. Alberts B, Johnson A, Lewis J, Raff M, Roberts K, Walter P. Molecular Biology of the Cell. 4th edition. New York: Garland Science; 2002.
38. Li W, Cowley A, Uludag M, Gur T, McWilliam H, Squizzato S, Park YM, Buso N, Lopez R. The EMBL-EBI bioinformatics web and programmatic tools framework. Nucleic Acids Res. 2015;43(W1):W580–W584. doi:10.1093/nar/gkv279.
39. Mehrotra S, Bg PK, Nayak PG, Joseph A, Manikkath J. Recent progress in the oral delivery of therapeutic peptides and proteins: overview of pharmaceutical strategies to overcome absorption hurdles. Adv Pharm Bull. 2023;14(1):11–33. doi:10.34172/apb.2024.009.

40. Ranjith D, Ravikumar C. SwissADME predictions of pharmacokinetics and drug-likeness properties of small molecules present in Ipomoea mauritiana Jacq. J Pharmacogn Phytochem. 2019;8(5):2063–2073.
41. Jendele L, Krivak R, Skoda P, Novotny M, Hoksza D. PrankWeb: a web server for ligand binding site prediction and visualization. Nucleic Acids Res. 2019;47(W1):W345–W349. doi:10.1093/nar/gkz424.
42. Binkowski TA, Naghibzadeh S, Liang J. CASTp: Computed atlas of surface topography of proteins. Nucleic Acids Res. 2003;31(13):3352–3355. doi:10.1093/nar/gkg512.
43. Ayaz E, Alpsoy HC. garlic (Allium sativum) and traditional medicine. Turkiye Parazitolojii Dergisi. 2007;31(2):145–149.
44. Tesfaye A. Revealing the therapeutic uses of garlic (Allium sativum) and its potential for drug discovery. Sci World J. 2021;2021(1):8817288. doi:10.1155/2021/8817288.
45. Shang A, Cao SY, Xu XY, Gan RY, Tang GY, Corke H, Mavumengwana V, Li HB. Bioactive compounds and biological functions of garlic (Allium sativum L.) Foods. 2019;8(7):246. doi:10.3390/foods8070246.
46. Bayan L, Koulivand PH, Gorji A. Garlic: a review of potential therapeutic effects. Avicenna J Phytomed. 2014;4(1):1–14.
47. Batiha GES, Beshbishy AM, Wasef LG, Elewa YHA, Al-Sagan AA, El-Hack MEA, Taha AE, et al. Chemical constituents and pharmacological activities of garlic (Allium sativum L.): A review. Nutrients. 2020;12(3):872. doi:10.3390/nu12030872.
48. Iciek M, Kwiecień I, Chwatko G, Sokołowska-Jeżewicz M, Kowalczyk-Pachel D, Rokita H. The effects of garlic-derived sulfur compounds on cell proliferation, caspase 3 activity, thiol levels and anaerobic sulfur metabolism in human hepatoblastoma HepG2 cells. Cell Biochem Funct. 2012;30(3):198–204. doi:10.1002/cbf.1835.
49. Diantini A, Subarnas A, Lestari K, Halimah E, Susilawati Y, Supriyatna, Julaeha E, Achmad TH, Suradji EW, Yamazaki C, Kobayashi K, Koyama H, Abdulah R. Kaempferol-3-O-rhamnoside isolated from the leaves of Schima wallichii Korth. inhibits MCF-7 breast cancer cell proliferation through activation of the caspase cascade pathway. Oncol Lett. 2003;3(5):1069–1072. doi:10.3892/ol.2012.596.
50. Tsiklauri L, An G, Ruszaj DM, Alaniya M, Kemertelidze E, Morris ME. Simultaneous determination of the flavonoids robinin and kaempferol in human breast cancer cells by liquid chromatography-tandem mass spectrometry. J Pharm Biomed Anal. 2011;55(1):109–113. doi:10.1016/j.jpba.2010.12.021.
51. Yi X, Zuo J, Tan C, Xian S, Luo C, Chen S, Yu L, Luo Y. Kaempferol, a flavonoid compound from Gynura Medica induced apoptosis and growth inhibition in Mcf-7 breast cancer cell. Afr J Tradit Complement Altern Med. 2016;13(4):210–215. doi:10.21010/ajtcam.v13i4.27.
52. Roy N, Davis S, Narayanankutty A, Nazeem PA, Babu TD, Abida PS, Raghavamenon A. Garlic phytocompounds possess anticancer activity by specifically targeting breast cancer biomarkers-an in-silico study. Asian Pac J Cancer Prev. 2016;17(6):2883–2888. doi:APJCP.2016.17.6.2883.
53. Odubela OO, Omirin ES, Olanrewaju AJ, Olugbogi EA, Aribisala PO, Nwachukwu KC, Okoh EF, Blessed SN, Boboye SO. Identification of antagonists of pro-survival Bcl-2 from Morus alba in human malignancies: An in-silico approach. Scicom J Med Appl Med Sci. 2024;3(1):36–44. doi:10.54117/sjmams.v3i1.15.
54. Pan Y, Zheng YM, Ho WS. Effect of quercetin glucosides from Allium extracts on HepG2, PC-3 and HT-29 cancer cell lines. Oncol Lett. 2018;15(4):4657–4661. doi:10.3892/ol.2018.7893.
55. Ward AB, Mir H, Kapur N, Gales DN, Carriere PP, Singh S. Quercetin inhibits prostate cancer by attenuating cell survival and inhibiting anti-apoptotic pathways. World J Surg Oncol. 2018;16(1). doi:10.1186/s12957-018-1400-z.
56. Nam JS, Sharma A, Nguyen L, Chakraborty C, Sharma G, Lee SS. Application of bioactive quercetin in oncotherapy: From nutrition to nanomedicine. Mol. 2016;21(1):108. doi:10.3390/molecules21010108.

57. Liu S, Matsuo T, Miyaji M, Hosoya O. Key pathways and genes influenced by a drug, NK-4, in human neurons. Invest Ophthalmol Vis Sci. 2018;59(9):6051.
58. Khan I, Bahuguna A, Kumar P, Bajpai VK, Kang SC. In vitro and in vivo antitumor potential of carvacrol nanoemulsion against human lung adenocarcinoma A549 cells via mitochondrial mediated apoptosis. Sci Rep. 2018;8(1). doi:10.1038/s41598-017-18644-9.
59. Imran M, Aslam M, Alsagaby SA, Saeed F, Ahmad I, Afzaal M, Arshad MU, Abdelgawad MA, El-Ghorab AH, Khames A, Shariati MA, Ahmad A, Hussain M, Imran A, Islam S. Therapeutic application of carvacrol: A comprehensive review. Food Sci Nutr. 2022;10(11):3544–3561. doi:10.1002/fsn3.2994.
60. Fatima K, Luqman S, Meena A. Carvacrol arrests the proliferation of hypopharyngeal carcinoma cells by suppressing ornithine decarboxylase and hyaluronidase activities. Front Nutr. 2022;9:857256. doi:10.3389/fnut.2022.857256.
61. Herrera-Calderon O, Yepes-Pérez AF, Quintero-Saumeth J, Rojas-Armas JP, Palomino-Pacheco M, Ortiz-Sánchez JM, Andía-Ayme V. Carvacrol: An in silico approach of a candidate drug on HER2, PI3Kα, mTOR, hER-α, PR, and EGFR receptors in the breast cancer. Evid Based Complement Alternat Med. 2020;1–12. doi:10.1155/2020/8830665.
62. Zari AT, Zari TA, Hakeem KR. Anticancer properties of eugenol: A review. Mol. 2021;26(23):7407. doi:10.3390/molecules26237407.
63. Yoo CB, Han KT, Cho KS, Ha J, Park HJ, Nam JH, Lee KT. Eugenol isolated from the essential oil of Eugenia caryophyllata induces a reactive oxygen species-mediated apoptosis in HL-60 human promyelocytic leukemia cells. Cancer Lett. 2005;225(1):41–52. doi:10.1016/j.canlet.2004.11.018.
64. Nazreen S, Elbehairi SEI, Malebari AM, Alghamdi N, Alshehri RF, Shati AA, Ali NM, Alfaifi MY, Elhenawy AA, Alam MM. New natural eugenol derivatives as antiproliferative agents: Synthesis, biological evaluation, and computational studies. ACS Omega. 2023;8(21):18811–18822. doi:10.1021/acsomega.3c00933.

